AFOSR-TR- 82-0367

TR-312

(13)

STUDY OF TURBULENT BOUNDARY LAYERS OVER ROUGH SURFACES, WITH EMPHASIS ON THE EFFECTS OF ROUGHNESS CHARACTER AND MACH NUMBER

Interim Report

by

M. L. Finson

February 1982

Sponsored by

Air Force Office of Scientific Research (AFSC)
United States Air Force

Under Contract No. F49620-80-C-0015

DTIC
ELECTE
MAY 6 1982
D
H

PHYSICAL SCIENCES INC.
30 COMMERCE WAY, WOBURN, MASS. 01801

(13)

TR-312

STUDY OF TURBULENT BOUNDARY LAYERS OVER ROUGH SURFACES, WITH EMPHASIS ON THE EFFECTS OF ROUGHNESS CHARACTER AND MACH NUMBER

Interim
[redacted] Report

by

M. L. Finson

February 1982

Sponsored by

Air Force Office of Scientific Research (AFSC)
United States Air Force

Under Contract No. F49620-80-C-0015

ACKNOWLEDGEMENT

This research was sponsored by the Air Force Office of Scientific Research (AFSC), United States Air Force, under Contract #F49620-80-C-0015. The United States Government is authorized to reproduce and distribute reprints for governmental purposes notwithstanding any copyright notation hereon.

UNCLASSIFIED
SECURITY CLASSIFICATION OF THIS PAGE (When Data Entered)

REPORT DOCUMENTATION PAGE	READ INSTRUCTIONS BEFORE COMPLETING FORM
1. REPORT NUMBER AFOSR-TR- 82-0367 2. GOVT ACCESSION NO. AD-A11	3. RECIPIENT'S CATALOG NUMBER 4217
4. TITLE (and Subtitle) Study of Turbulent Boundary Layers over Rough Surfaces, with Emphasis on the Effects of Roughness Character and Mach Number	5. TYPE OF REPORT & PERIOD COVERED INTERIM (ANNUAL) 1 NOV 80 - 30 SEP 81 6. PERFORMING ORG. REPORT NUMBER
AUTHOR(s) M. L. Finson	8. CONTRACT OR GRANT NUMBER(s) F49620-80-C-0015
PERFORMING ORGANIZATION NAME AND ADDRESS PHYSICAL SCIENCES INC. 30 Commerce Way Woburn, MA 01801	10. PROGRAM ELEMENT, PROJECT, TASK AREA & WORK UNIT NUMBERS 61102F 2307/A1
11. CONTROLLING OFFICE NAME AND ADDRESS Air Force Office of Scientific Research/NA Bolling AFB, D.C. 20332	12. REPORT DATE February 1982 13. NUMBER OF PAGES 72
14. MONITORING AGENCY NAME & ADDRESS (if different from Controlling Office)	15. SECURITY CLASS. (of this report) Unclassified 15a. DECLASSIFICATION/DOWNGRADING SCHEDULE

16. DISTRIBUTION STATEMENT (of this Report)

Approved for public release; distribution unlimited.

17. DISTRIBUTION STATEMENT (of the abstract entered in Block 20, if different from Report)

18. SUPPLEMENTARY NOTES

19. KEY WORDS (Continue on reverse side if necessary and identify by block number)

Turbulent Boundary Layers
Turbulent Heat Transfer
Re-entry Heating

20. ABSTRACT (Continue on reverse side if necessary and identify by block number)

A Reynolds stress model for turbulent boundary layers on rough walls is used to investigate the effects of roughness character and compressibility. The flow around roughness elements is treated as form drag. A method is presented for deriving the required roughness shape and spacing from profilometer surface measurements. Calculations based on the model compare satisfactorily with low speed data on roughness character and hypersonic measurements with grit roughness

The computer model is exercised systematically over a wide range of parameters to derive a practical scaling law for the equivalent roughness. In contrast to previous correlations, for most roughness element shapes the effective roughness is not predicted to show a pronounced maximum as the element spacing decreases. The effect of roughness tends to be reduced with increasing edge Mach number, primarily due to decreasing density in the vicinity of the roughness elements. It is further shown that the required roughness Reynolds number for fully rough behavior increases with increasing Mach number, explaining the small roughness effects observed in some hypersonic tests.

ABSTRACT

A Reynolds stress model for turbulent boundary layers on rough walls is used to investigate the effects of roughness character and compressibility. The flow around roughness elements is treated as form drag. A method is presented for deriving the required roughness shape and spacing from profilometer surface measurements. Calculations based on the model compare satisfactorily with low speed data on roughness character and hypersonic measurements with grit roughness. The computer model is exercised systematically over a wide range of parameters to derive a practical scaling law for the equivalent roughness. In contrast to previous correlations, for most roughness element shapes the effective roughness is not predicted to show a pronounced maximum as the element spacing decreases. The effect of roughness tends to be reduced with increasing edge Mach number, primarily due to decreasing density in the vicinity of the roughness elements. It is further shown that the required roughness Reynolds number for fully rough behavior increases with increasing Mach number, explaining the small roughness effects observed in some hypersonic tests.

TABLE OF CONTENTS

LIST OF FIGURES

LIST OF FIGURES (CONT.)

LIST OF FIGURES

1. INTRODUCTION

Surface roughness can play an important role in increasing friction and heat transfer under turbulent boundary layer conditions. Roughness effects have been studied extensively over the past fifty years, in connection with applications such as head losses in pipes and other hydraulic equipment, ship hull drag, airplane drag, and high speed missile drag and heating. This study emphasizes the effects of roughness character and the behavior of rough-wall boundary layers under supersonic and hypersonic conditions. Hypersonic boundary layers tend to be quite thin, which naturally increases the likelihood that roughness will be important. There have been few experimental or theoretical investigations of rough wall turbulent boundary layers at high Mach numbers. Furthermore, many high speed flight vehicles, such as re-entry vehicles, are fabricated from composite materials. Since these typically involve woven fibers filled with a resin, they present a different roughness character than would be found on, say, a metallic surface.

One cannot adequately discuss the behavior of flows over rough surfaces without recalling the classic experiments of Nikuradse,[1] in which water was flowed through pipes roughened by sand. In the "fully rough" regime, the measured friction factor λ was found to depend only on the ratio of roughness height k_s and pipe radius

$$\lambda = [1.74 + 2 \log_{10} R/k_s]^{-2} \quad . \qquad (1)$$

(A list of symbol definitions is given on page 61). This result holds for $k_s^+ = U_\tau k_s/\nu$ greater than about 70. Smooth wall behavior prevails for $k_s^+ < 5$, and Nikuradse presented a correlation for the intermediate transition regime. Analogous experiments were performed by Dipprey and Sabersky[2] to extend Nikuradse's results to heat transfer at various Prandtl numbers. Although Nikuradse's sand grains were carefully sifted to obtain a relatively uniform size (diameter = k_s), we have no detailed information on the statistics of the roughened surface that resulted from adhesively bonding the sand grains to the smooth surface.

Some very detailed measurements were obtained by Moffat and co-workers[3-5] on the low speed flow of air over a flat plate covered by closely packed spheres. Their data include skin friction, heat transfer, and profiles of mean and fluctuating quantities. These results are quite useful for validating theoretical models. However, only one roughness was investigated.

Another important class of experiments involves "two-dimensional" roughness, such as machined grooves or square rods, normal to the flow direction. Betterman[6] varied the relative rod spacing by a factor of about three, and Antonia and Luxton[7] made detailed surveys of the turbulence parameters in the boundary layer over this type of roughness. While several authors have correlated 2-D roughness data along with 3-D or distributed roughness data, 2-D roughness will not be considered here. We might expect substantial differences in the nature of the flows. With 2-D roughness, the flow is likely to be dominated by cavities in the grooves between elements, whereas separation should be less important with distributed roughness. The model presented below is aimed entirely at distributed roughness, appropriate to the vast majority of practical applications.

The available data base on roughness effects in compressible flows is considerably smaller than that for low speeds. The most extensive set of experiments were those of the Passive Nosetip Technology (PANT) program,[8] in which roughened hemispherical models were placed in NSWC Tunnel 8 at a freestream Mach number $M_\infty = 5$. Heat transfer was measured by calorimeter methods. The roughness, which varied over two orders of magnitude in height, was created by grit blasting or by bonding grit particles; a considerable quantity of data were obtained on both roughness augmentation of turbulent heating as well as roughness-induced transition. It should be emphasized that these tests were performed on blunt nose regions, where the boundary layer edge Mach numbers are subsonic or modestly supersonic. While there is a substantial variation of density and temperature across the boundary layer in these conditions, they certainly are not representative of high Mach number boundary layers.

Holden[9] has run tests in the hypersonic shock tunnel at Calspan (M_∞ = 11-13) on 45° cones to which grit was bonded; the boundary layer edge Mach number is about 1.8. Higher edge Mach numbers, about 4.8, were obtained in NSWC Tunnel 2 by Keel,[10] on 5° cones with sand grains attached by epoxy.

In the same facility, Voisinet[11] measured the combined effects of roughness and mass addition. He created the roughness by covering a porous section of the tunnel wall with a screen. This provides a questionable simulation of distributed roughness, but is undoubtedly necessitated by the extreme difficulty in fabricating a rough porous surface with controlled permeability.

Truly hypersonic tests have been performed by Hill[12] (NSWC Hypervelocity Tunnel) and Holden[13] (Calspan hypersonic shock tunnel), using grit bonded to the surface of slender cones. Hill's experiments, on a 7° cone at $M_e = 8.1$, used three different roughness heights. Holden employed a single roughness on a 6° cone but introduced varying angles of attack to thin the boundary layer on the windward side, effectively increasing the roughness effect ($M_e = 4.4 - 9.4$). Despite the general similarity of the conditions for these two experiments, there are differences in the results that deserve further discussion below.

Investigations on the effects of roughness character, where the shape and spacing of roughness elements are varied, are rather limited. The classic experiment was performed by Schlichting,[14] on one wall of a water channel. Various arrangements of roughness elements were used, including spheres, spherical segments, cones, and short angles, at several relative spacings. Results were presented in terms of the wall shear and equivalent sand grain roughnesses. Several others have investigated the roughness character effect over more limited ranges, mostly by changing the spacing for a given shape. Chen and Roberson[15] studied three relative spacings of hemispheres, for air flow through a pipe. Raupach, Thom and Edwards[16] varied the relative spacing over a factor of four for cylindrical elements ($k/D = 1$) in a wind tunnel. In water channel flume experiments, Mirajgaoker and Charlu[17] used stones at six spacings and Sayre and Albertson[18] used baffles (similar to Schlichting's short angles, but with width = 4 × height), again with six spacings. O'Loughlin and Annambhotla[19] used cubes at three spacings, in a wind tunnel. Mulhearn and Finnigan[20] examined gravel at one spacing in a wind tunnel. To simulate plant crop canopy flow, Thom[21] and Seginer et al.[22] studied tall, thin rods ($k/D \sim 100$), which provide a major variation in aspect ratio of the roughness elements.

One series of roughness character tests under supersonic conditions has recently been conducted by Acurex Corp.[23] in AEDC Tunnel F. The models were 45° cones, with an edge Mach number of 1.7. Seven surfaces were used: essentially smooth, grit blasted, bonded grit, and four chemically-etched roughness patterns (two heights, two spacings each). The accuracy of the measured heating rates may be limited by the fact that Tunnel F was an arc heated, hot-shot type, with pressure decreasing continuously during the test time, and by the fact that the roughness characteristics varied over the model surface.

A great number of methods of varying degrees of empiricism have been developed to predict rough wall drag and heating. The soundest methods start with Nikuradse's observation that the logarithmic portion of the mean velocity is shifted downward by roughness. This downward shift, $\Delta U_1/U_\tau$, is also directly related to the roughness-induced increase in friction by the following relation (at least for low speed flows)

$$\left(\frac{2}{C_f}\right)^{1/2} = \left(\frac{2}{C_{f_{sm}}}\right)^{1/2} - \frac{\Delta U_1}{U_\tau} \quad . \tag{2}$$

The velocity shift depends on wall conditions, and thus is a function only of k^+. The smooth wall friction coefficient generally depends on the Reynolds number based on some measure of the thickness of the viscous zone (e.g. Re_θ), as well as on pressure gradient and other geometrical factors (boundary layer vs. pipe, etc.). In the fully rough regime, however, the dependence of $C_{f_{sm}}$ on Re_θ combines with dependence of $\Delta U_1/U_\tau$ on k^+ to yield a dependence only on the ratio k/θ (or k/R in a pipe), independent of Reynolds number. Note that Eq. (2) is transcendental in C_f, since k^+ involves $U_\tau = \sqrt{\tau_w/\rho_w}$. Also, the above equation cannot be applied directly to compressible flows.

For sand grain roughness, the velocity shift in the fully rough regime is

$$\frac{\Delta U_1}{U_\tau} = 5.6 \log k_s^+ - 3 \quad . \tag{3}$$

Dvorak[24,25] first extended this relation to describe variations in roughness character

$$\frac{\Delta U_1}{U_\tau} = 5.6 \log k^+ + f(\lambda) \quad , \tag{4}$$

so that the equivalent sand grain roughness (k_s) is related to the actual roughness height (k) by

$$5.6 \log k_s/k = f(\lambda) + 3 \; . \tag{5}$$

Here $f(\lambda)$ is some measure of the roughness density. Dvorak correlated the available data with λ^{-1} being the fraction of the surface covered by roughness (the base area of roughness elements per unit underlying smooth surface area). Simpson[26] obtained improved results in terms of λ_k, the inverse of the projected frontal area of the elements per unit surface area, and others[27,28] have used similar variations of the Dvorak approach.

Figure 1 shows Simpson's roughness density correlations. The two straight line segments are the same as Dvorak's (in terms of λ rather than λ_k). Note that the roughness effect has a maximum at $\lambda_k = 4.70$, which corresponds to spherical elements with an average separation of 1.9 diameters. Note also that nearly all of the data to the left of this maximum, for more closely packed elements, are for two-dimensional roughness. Simpson notes that the flow in this regime may be dominated by cavity flow between the elements, and speculates that this decrease in roughness effect with decreasing spacing may not occur for 3-D roughness. We shall return to this matter in some depth below.

For compressible flows, Dvorak[25] applied the same compressibility factor used for smooth walls (these are surveyed in Ref. 29). Equation (2) is

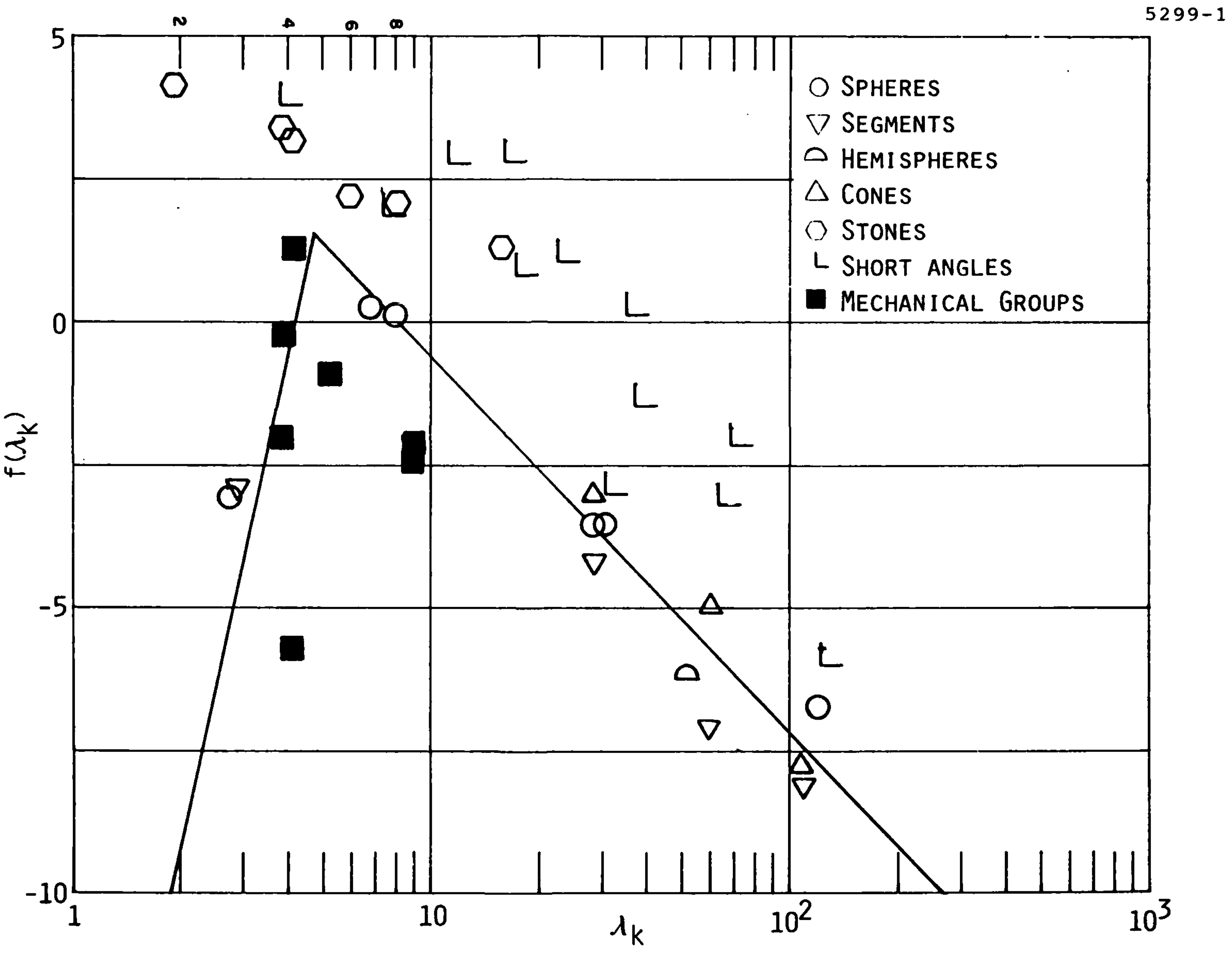

Fig. 1 Simpson's correlation for the effect of roughness density.[26]

used to compute an incompressible friction coefficient, with $C_{f_{sm}}$ based on $F_\theta \cdot Re_\theta$ and $\Delta U_1/U_\tau$ based on the actual wall conditions; the compressible friction coefficient is then obtained by dividing the incompressible value by F_C. However, this procedure is not necessarily logically consistent with the incompressible behavior. If $\Delta U_1/U_\tau$ really depends on local wall conditions, then Eq. (2) would apply directly to compressible situations, simply by inserting the appropriate compressible value of $C_{f_{sm}}$. But Dvorak found this alternative to yield poor agreement with data.

A number of investigators have developed more empirical methods for reentry applications. One of these, which is well-known and has been derived from both low speed and high speed measurements, is the version developed by Acurex Corp. and contained in the ABRES Shape Change Code.[30] The roughness augmentation of skin friction is described by an influence coefficient, by which the smooth wall value should be multiplied, independent of compressibility:

$$
\begin{aligned}
I_f &= 1 + 0.5\, f_1(k/\theta) g_1(\chi) && (6)\\
f_1(k/\theta) &= 1 + 0.09\, k/\theta + 0.53(1-e^{-k/\theta}) &&\\
g_1(\chi) &= \chi + 1.5(1-e^{-\chi}) \qquad \text{for } \chi > 0 &&\\
&= 0 \qquad \text{for } \chi < 0 &&\\
\chi &= \log(k^+/15.5) \ \text{(Based on smooth wall } C_f\text{).} &&
\end{aligned}
$$

While this relation provides a smooth transition between smooth and rough wall behavior, it does not obviously reduce to the dependence observed by Nikuradse in the fully rough regime, in that the drag is predicted to depend on both k^+ and k/θ. Dahm[31] has recently developed a new correlation for roughness effects, involving a "two-layer" model.

Another issue of considerable uncertainty is the relation between heat transfer and skin friction. For smooth walls, the mechanisms of turbulent heat and momentum transfer are quite similar and the heat transfer and skin friction coefficients are closely related. But with rough walls, form drag on the elements has no analogous thermal mechanism. This provides an intuitive explanation for the common observation that roughness causes smaller increases in heating than in friction. Owen and Thompson[32] developed a correlation for roughness-dominated heat transfer, following lines suggested by assuming cavity flow between the elements. However, the result involves primarily k^+ and it is not clear whether this behavior is consistent with the well known dependence of skin friction on k/δ rather than k^+. The heat transfer correlation used in the ABRES Shape Change Code[30] is simple and pragmatic - the numerical factor 0.5 in Eq. (6) is replaced by 0.3.

The analyses to be presented below are based on a fairly basic model for rough wall boundary layers, wherein a Reynolds stress turbulence model is combined with a form drag description for the effect of roughness elements on the flow. The computer model is used in two ways; 1) it is compared against relevant data to establish the validity and accuracy of the theory and to offer explanations for observed trends; and 2) it is used to develop correlations for engineering applications by suggesting scaling laws and by providing numerical data to be correlated. In previous papers,[33,34] we showed comparisons with a good portion of the available measurements and presented some preliminary scaling laws. Here we will analyze some of the most important data on roughness character and compressibility, and shall present correlations that should have widespread utility.

2. ROUGH WALL BOUNDARY LAYER MODEL

The basic model for rough wall turbulent boundary layers is the same as that used previously,[33,34] and we shall only outline the most relevant features here. The turbulence model is a Reynolds stress or second-order closure method, which computes both mean and fluctuating velocities and temperatures. The dependent velocity variables are the mean velocity vector U_i, the Reynolds stress tensor $\overline{u_i'u_j'}$, and the isotropic dissipation rate Φ. The analogous thermal variables (temperature or, more precisely, enthalpy h) are the mean enthalpy $\bar{h}$, the mean square fluctuating enthalpy $\overline{h'^2}$, and the Reynolds heat flux vector $\overline{u_i'h'}$. Under the boundary layer approximation, this set of variables reduces to U, V, $\overline{u'^2}$, $\overline{v'^2}$, $\overline{w'^2}$, $\overline{u'v'}$, Φ, $\bar{h}$, $\overline{h'^2}$, $\overline{u'h'}$, and $\overline{v'h'}$. The closure approximations that are used to derive the required equations are somewhat standard at this time. The formulation has been successfully applied to a variety of smooth wall boundary layer and free shear flows. Predicted smooth wall skin friction coefficients are generally within 10-15% of accepted values, except for a few cases with very large density differences, to be noted below.

Our model makes the basic assumption that the force on roughness elements can be viewed as form drag. This implicitly requires that the flow approaching an individual element be attached. As already noted, cavity flow is likely to prevail with 2-D roughness; for this reason the present model should be more appropriate for distributed roughness.

The rough surface is idealized as being made up of identical elements (although the extension to a size distribution would be straightforward). The bottom of the elements, or the underlying smooth wall, is at y=0. The element height is k, and ℓ is the average element spacing (ℓ^{-2} gives the number of elements per unit area). We restrict our treatment to elements with circular cross sections at all heights, with D(y) denoting the diameter at height y ($y < k$). As discussed in more detail in Ref. 33, form drag on the elements is described by an appropriate negative (sink) term in the mean momentum equation:

$$R_u = -\frac{1}{2}\rho U^2 C_D\, D(y)/\ell^2 \ . \qquad (7)$$

A drag coefficient value of $C_D = 0.6$ is roughly appropriate for elements such as cones or hemispheres. In addition, there should be source terms for turbulent kinetic energy and dissipation, describing the tendency of roughness to increase velocity fluctuations. These terms, which are discussed in Ref. 33, are not very important compared to the indirect effect of roughness to increase the turbulent energy by increasing the mean shear.

Except in the Stokes flow regime, heat transfer to an element should be small. Therefore, the only roughness term appearing in the thermal equations is a source term for the mean static enthalpy. This term is constructed so that, in combination with Eq. (7), form drag does not alter total enthalpy.

$$R_h = + 1/2 \rho U^3 C_D D(y)/\ell^2 \quad . \tag{8}$$

It is also necessary to account for the blockage effect of the roughness elements. At a given height, the fraction of the flow area normal to the x direction is $1-D(y)/\ell$. Terms that act in the streamwise direction, such as the convective operator $\rho U \partial/\partial x$, are multiplied by this factor. Terms that act on planes normal to the y direction, or that act on a unit volume, should be modified by $1-\pi D^2/4\ell^2$. However, the roughness terms discussed above are already based on the total volume, rather than the available flow volume, and need no such factor. If the entire equation is divided by $B(y) = 1-\pi D^2/4\ell^2$, a relatively simple result is obtained. For example, the mean momentum equation becomes

$$f(y)\rho u \frac{\partial U}{\partial x} + \rho V \frac{\partial U}{\partial y} = - f(y) \frac{\partial p}{\partial x} + \frac{1}{B} \frac{\partial}{\partial y} B\mu \frac{\partial U}{\partial y} - \frac{\partial}{\partial y} (\overline{\rho u'v'}) - \frac{1}{2} \rho U^2 C_D \frac{D}{\ell^2} B^{-1} \tag{9}$$

where

$$f(y) = \frac{1-D/\ell}{1-\pi D^2/4\ell^2} \qquad (10)$$

The function f(y) contains the main effect of blockage and may be absorbed in the definition of the stream function that is introduced to eliminate the normal velocity

$$\frac{\partial\psi}{\partial y} = f(y)\rho U \ , \ \frac{\partial\psi}{\partial x} = - \rho V \quad . \qquad (11)$$

Note that if the elements are packed so tightly that they are touching over some range of y, then $D = \ell$ and $f(y) = 0$ over that range. Our formulation forces the velocity to remain zero up to the height where $D < \ell$ and the flow is unblocked. Of course, common sense would dictate redefining $y = 0$ as the lowest point where the flow is unblocked.

A major advantage of this model is that solutions are obtained for both velocity and thermal variables. Heat transfer is obtained directly, without invoking a Reynolds analogy. Finite difference solutions are obtained using the obvious boundary conditions. Fluctuating quantities are zero at the base of the wall, $y = 0$. At the outer edge, fluctuating quantities are zero for a boundary layer or obey a symmetry condition for a channel flow. For numerical solutions, the equations are first transformed to the stream function coordinate, guaranteeing mass conservation and eliminating the normal velocity, V.

The transverse coordinate is normalized by the edge value of the stream function so that additional mesh points need not be carried in the free stream to allow for boundary layer growth. For proper resolution of the region near the wall, a linear mesh in the logarithm of the stream function is used. The finite-difference equations are solved with a block tridiagonal Newton-Raphson technique.

It should be noted that the use of such a model is not unique to this study. Lin and Bywater[35] have used the present form drag treatment in a two-equation TKE model, and generally obtained results superior to those obtained from lower level approaches. A very similar model has been developed by Wilson and Shaw[36] to analyze transport processes in plant canopies. A crop of corn plants, or a stand of trees, represents an attractive geometry for the form drag model. For such applications, it may be necessary to account for the effect of plant motion on the turbulent energy budget.

3. SPECIFICATION OF ROUGHNESS CHARACTERISTICS

An important aspect of predicting or analyzing roughness effects is the proper specification of the roughness characteristics. For laboratory experiments in which identical elements of a simple shape (spheres, cones, etc.) are attached to a smooth surface in a regular pattern, the required element height, shape and average spacing are obvious. Such is not necessarily the case for grains of sand or grit, sifted to a narrow size range and applied to the surface with an adhesive. The details of the bonding technique and the departure from sphericity of the particles can affect the roughness parameters. Real surface materials introduce even greater uncertainties. Here we present the method for deriving the roughness specifications, required for our model, from profilometer surface measurements.

A profilometer measurement of the surface in question is required. This consists of an irregular trace of height y, above some reference, as a function of distance along the line over which the stylus was traced. It will be assumed here that all elements are identical in size and shape - one could derive a more sophisticated analysis for situations where a significant variation in element sizes is expected. It is also assumed that location of roughness elements has at least a moderate degree of randomness.

Figure 2 sketches a typical profilometer curve. From this curve, it is necessary to form a probability of exceedance distribution, P.E.(y), which is simply the fraction of the trace with heights greater than y. One must also identify peaks and compute the average spacing between peaks, L_p. Finally, one must define the height y = 0, corresponding to the effective floor of the roughness.

Now, any element located within a roughness element base radius on either side of the profilometer line should be detected and counted as a peak. Since ℓ^{-2} is the number of elements per unit area, a profilometer trace of length L_t should detect $D(0)L_t/\ell^2$ peaks. The number detected is L_t/L_p, by definition of the average peak spacing. Equating these two quantities gives

$$\ell^2 = D(0)L_p \ . \qquad (12)$$

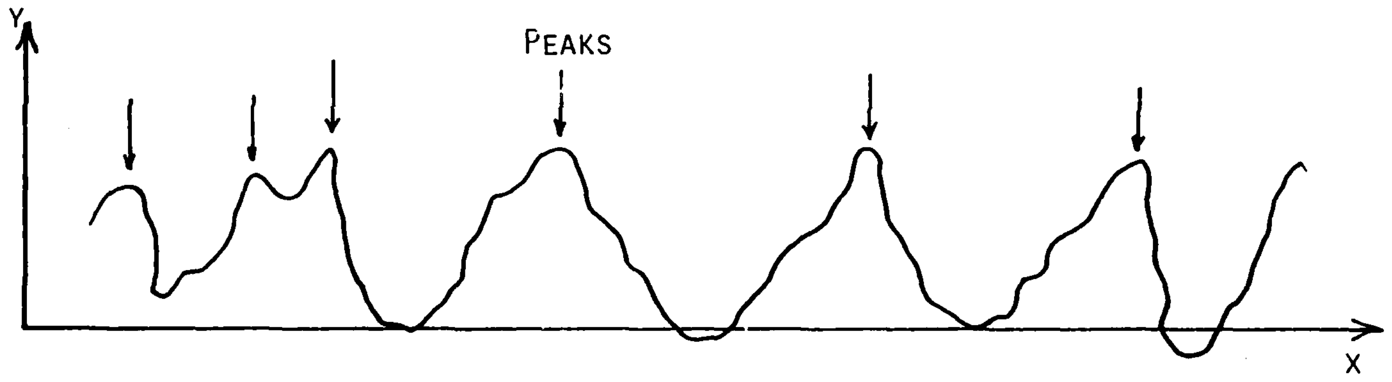

Fig. 2 Sketch of typical profilometer trace.

Since the roughness statistics are taken to be uniform, the probability of exceedance of height y along a profilometer trace must equal the fraction of the surface area above that height. The latter fraction is simply the cross-sectional area of an element at the height, $\pi/4\ D^2(y)$, multiplied by the density of elements, ℓ^{-2}.

$$P.E.(y) = \frac{\pi}{4} D^2(y)/\ell^2 \tag{13}$$

Equations (12) and (13) are sufficient to reconstruct the roughness characteristics. From the P. E. value at $y = 0$ (which should be less than $\pi/4$ to allow $D(0) < \ell$), Eqs. (12) and (13) yield $D(0)$ and ℓ. Equation (13) can then be used to obtain $D(y)$ for greater heights.

Some examples of the roughness specifications that result from this process will be given below, for grit-bonded surfaces. In practice, some judgement is required to identify the "floor" of the surface ($y = 0$) as well as to identify peaks in the profilometer curves. With sufficient statistics (e.g., the profilometer traces should intersect on the order of 100 or more elements), the practical effects of such uncertainties is small, because the portions of the elements near the base do not contribute greatly to the total drag.

4. COMPARISONS WITH ROUGHNESS CHARACTER DATA

As indicated in the Introduction, the most extensive experiment on roughness character is the Schlichting[14] study of various roughness patterns on one wall of a water channel. In Ref. 34 we made some preliminary analyses of Schlichting's data, using boundary layer solutions at the proper value of Re_δ. Here in Figs. 3-6, we show more appropriate solutions for the proper channel geometry.

For spheres, Fig. 3, the rough wall boundary layer model agrees acceptably with the measured friction coefficients, the worst error being about 25% at $\lambda_k = 3$ or $\ell/D \sim 1.5$. At the closest packing, we specified hemispheres, since the bottom half of spheres would be completely blocked. This is done for numerical convenience, to avoid singularities associated with $f(y) = 0$ in Eq. 9. According to our calculations, blockage of the bottom half-sphere is responsible for most of observed reduction in drag as $\ell/D \rightarrow 1$. For comparison, the Dvorak/Simpson correlations (which are identical for spheres) are also plotted.

For spherical segments, which are somewhat less than hemispheres, probably to simulate rivets, the computer code gives excellent results (Fig. 4). Note that the code shows only a very modest maximum in C_f, in contrast to the Dvorak and Simpson correlations. Good agreement was also obtained with Chen and Roberson's[15] data on hemispheres, although they investigated only very large roughness spacings.

For Schlichting's cones, shown in Fig. 5, our model is slightly low. Closely packed cones were not tested, but again the present model shows no pronounced peak. The short angles of Fig. 6 were simulated as cylinders of the same height and width in our calculations. The model is noticeably low here, for unknown reasons. However, we would expect less accuracy for cases with non-circular roughness, and similar errors would be expected for the baffles of Sayre and Albertson.[18] Generally good agreement was achieved with the data of Raupach, Thom and Edwards,[16] on cylinders (height ± diameter), as shown in Fig. 7.

Figure 8 compares our results with the observations of Mirajgaoker and Charlu.[17] We used the channel flow version of our model to simulate their

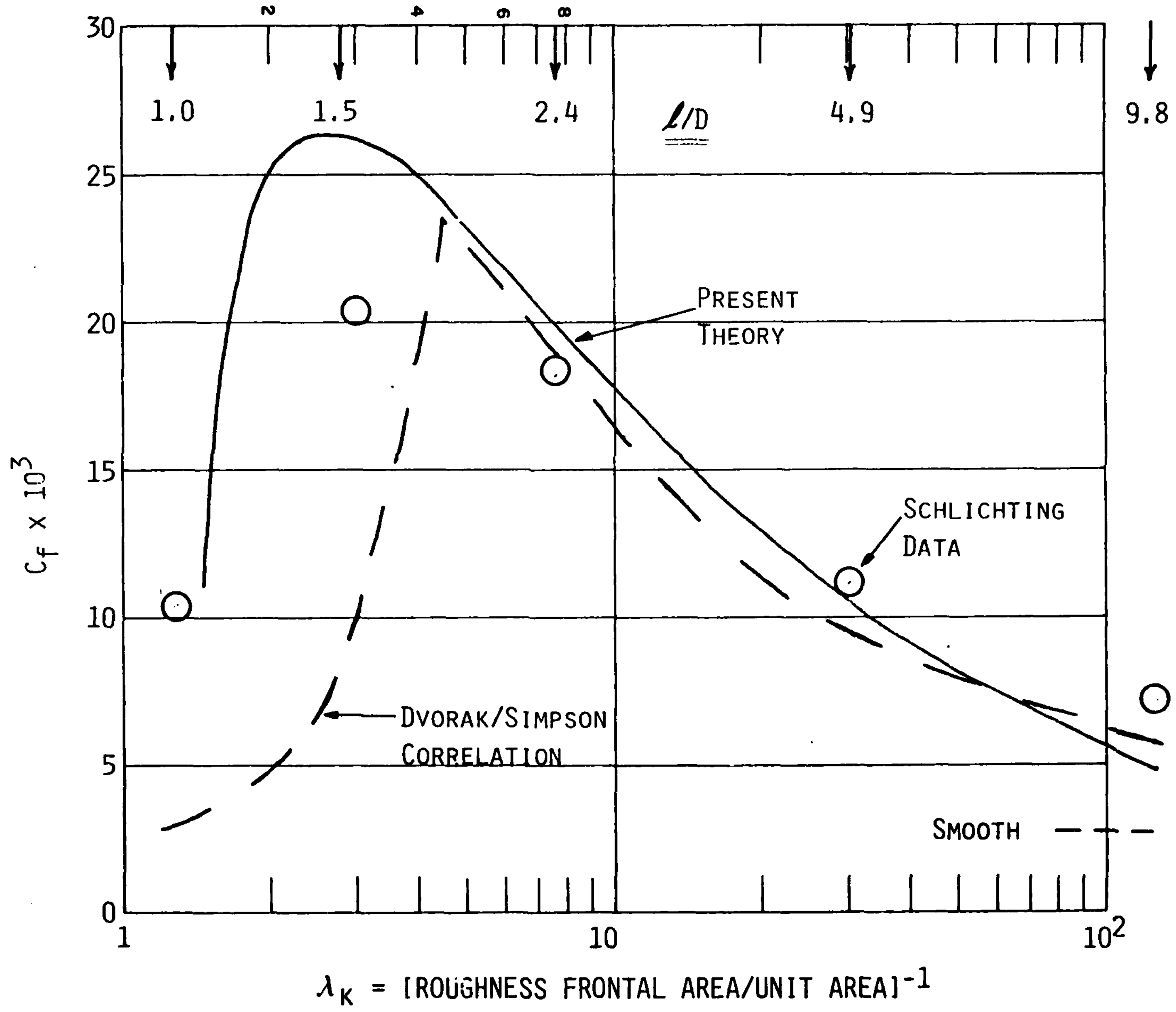

Fig. 3 Comparison of present model with Schlichting's[14] measurements for spherical roughness as a function of spacing.

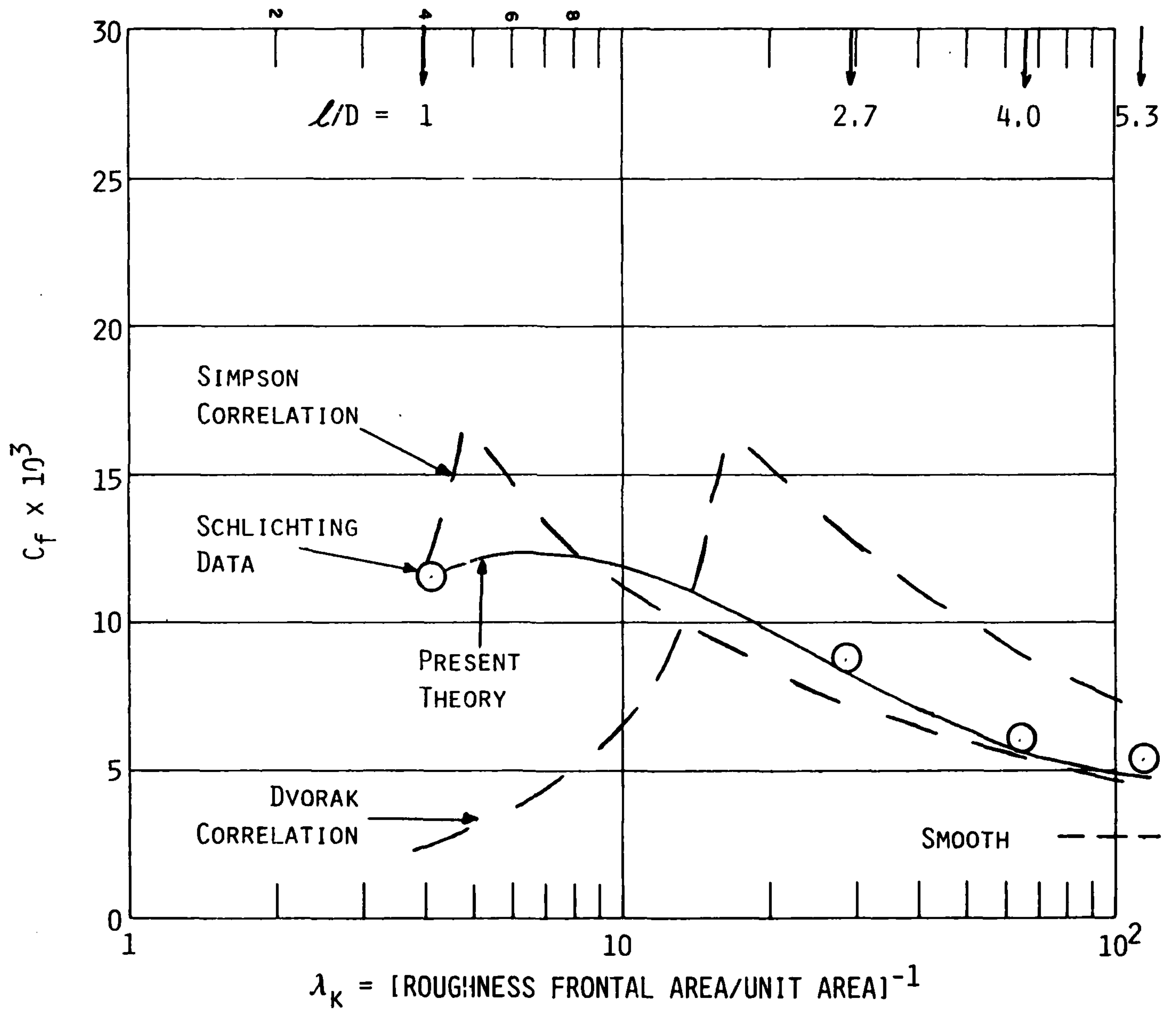

Fig. 4 Comparison of present model with Schlichting's[14] measurements for spherical segment roughness as a function of spacing.

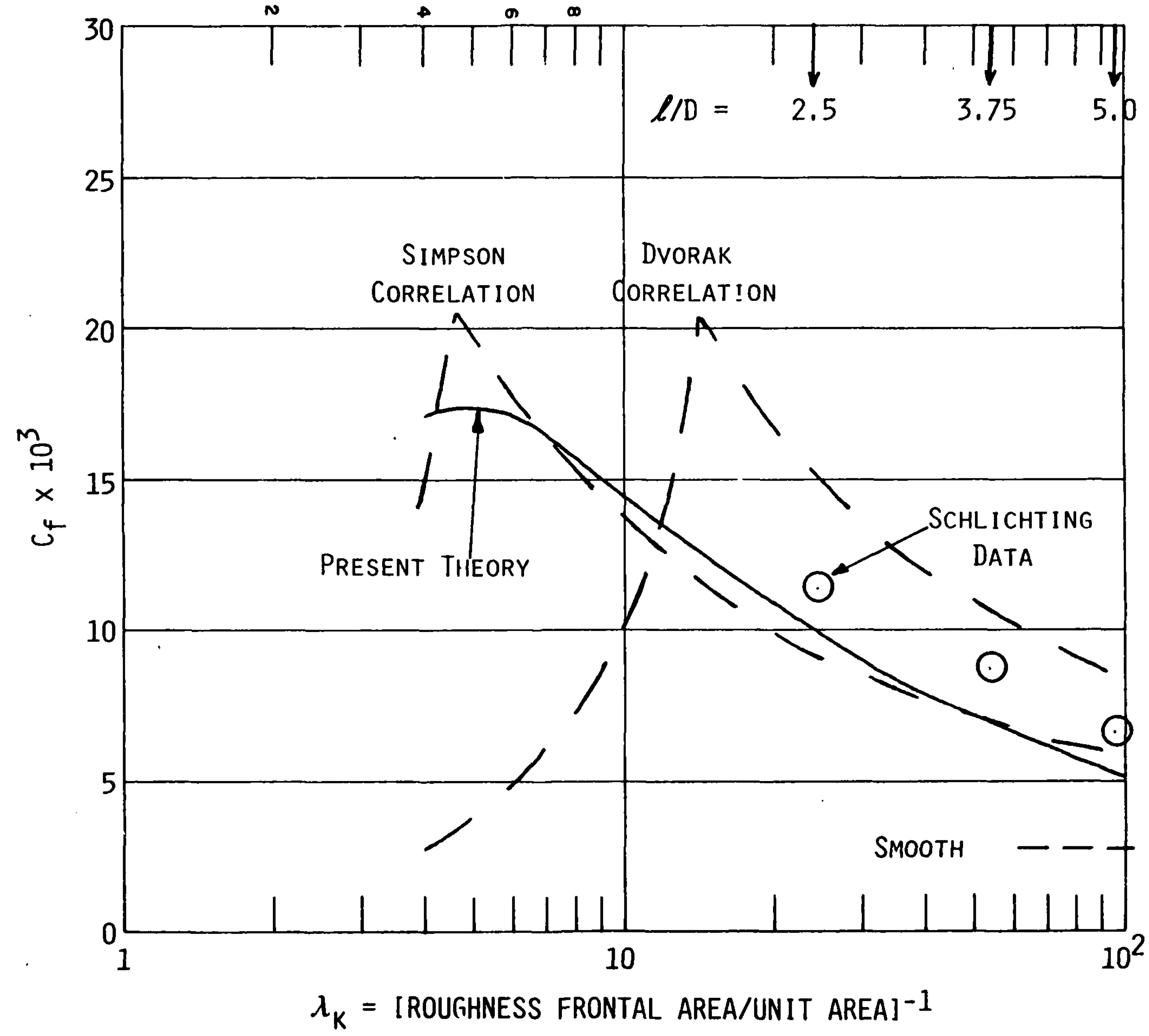

Fig. 5 Comparison of present model with Schlichting's[14] measurements for conical roughness as a function of spacing.

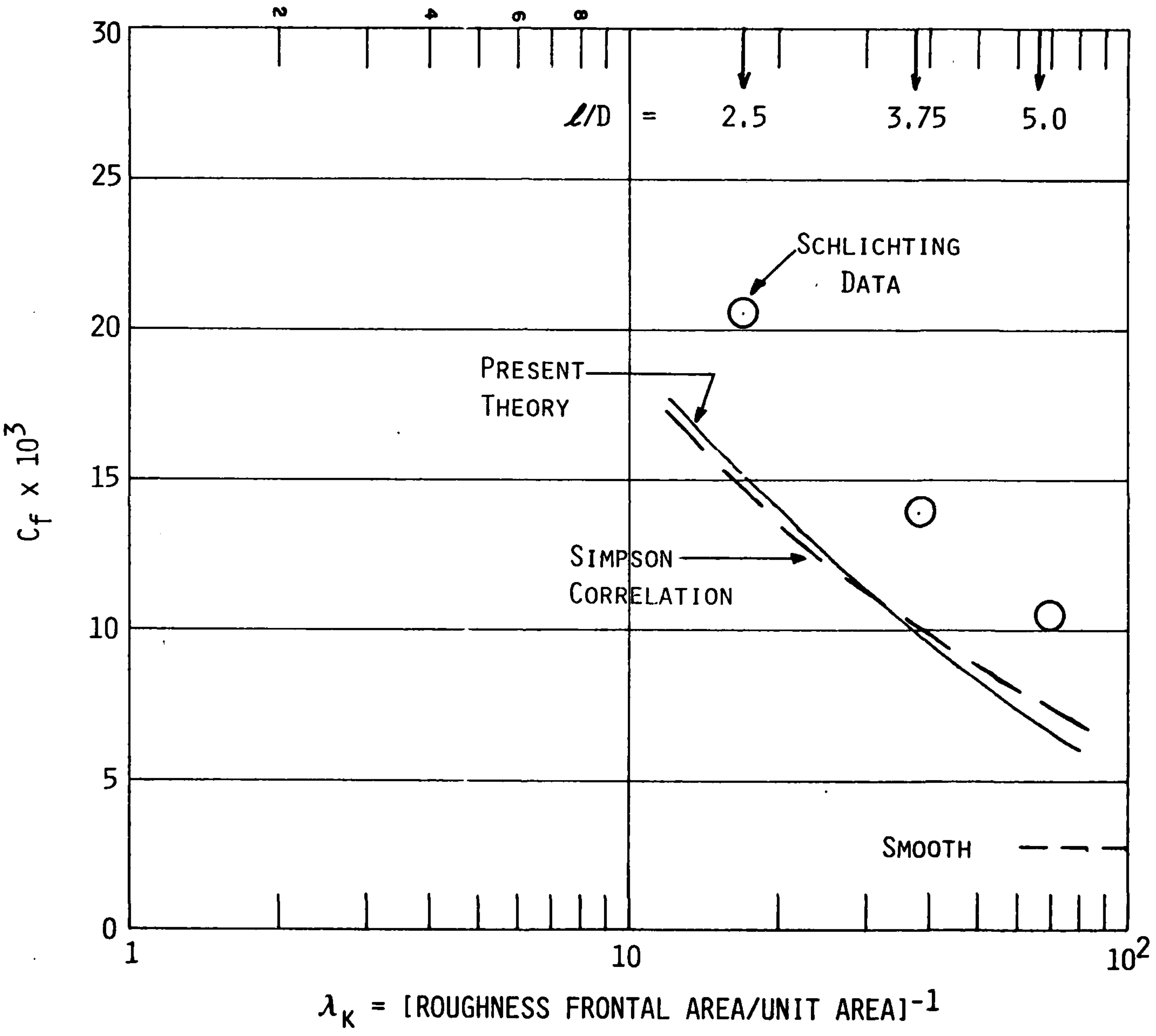

Fig. 6 Comparison of present model with Schlichting's[14] measurements for short angle roughness as a function of spacing.

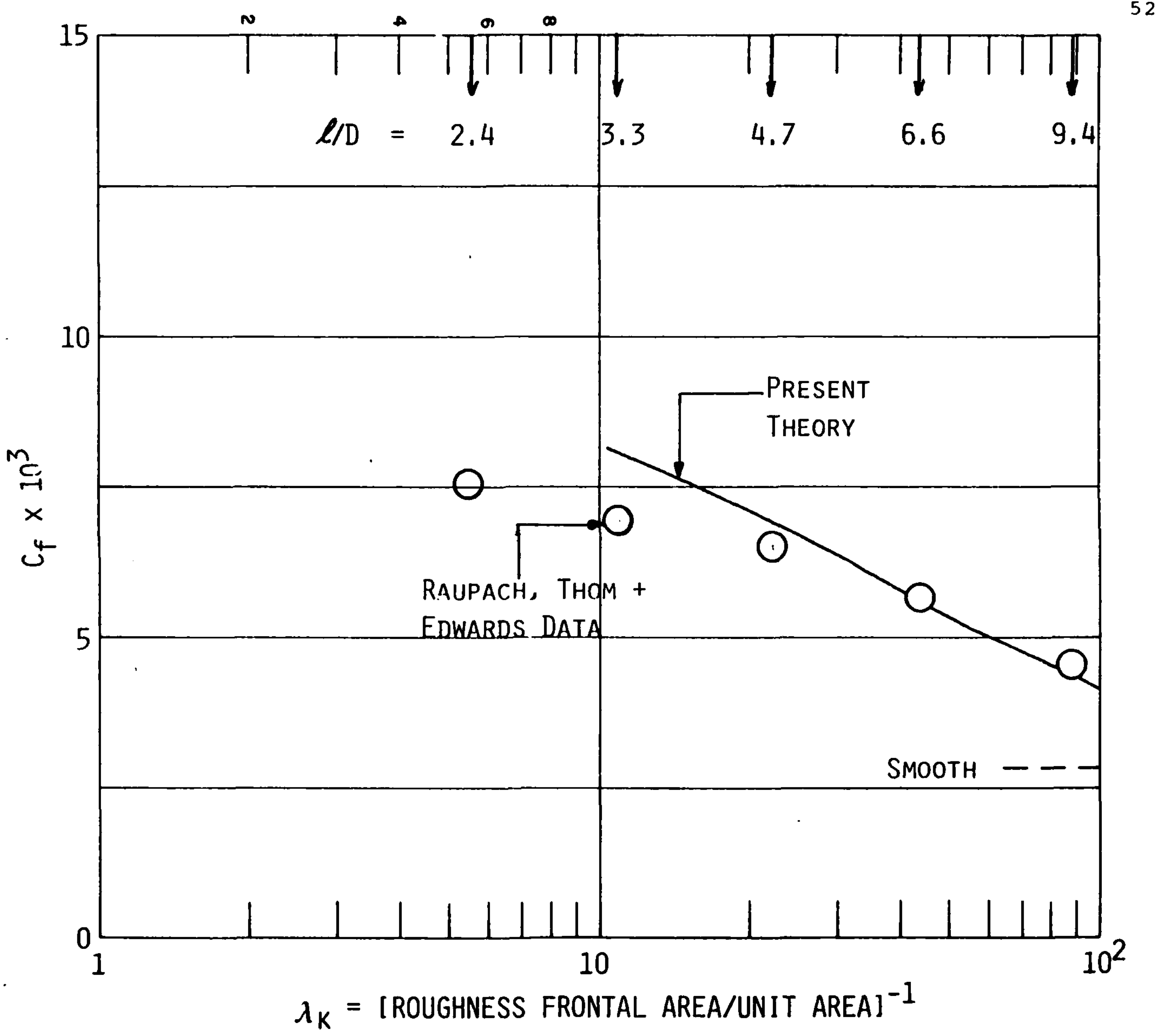

Fig. 7 Comparison of present model with the measurements of Raupach, Thom and Edwards[16] for cylindrical roughness elements at various spacings.

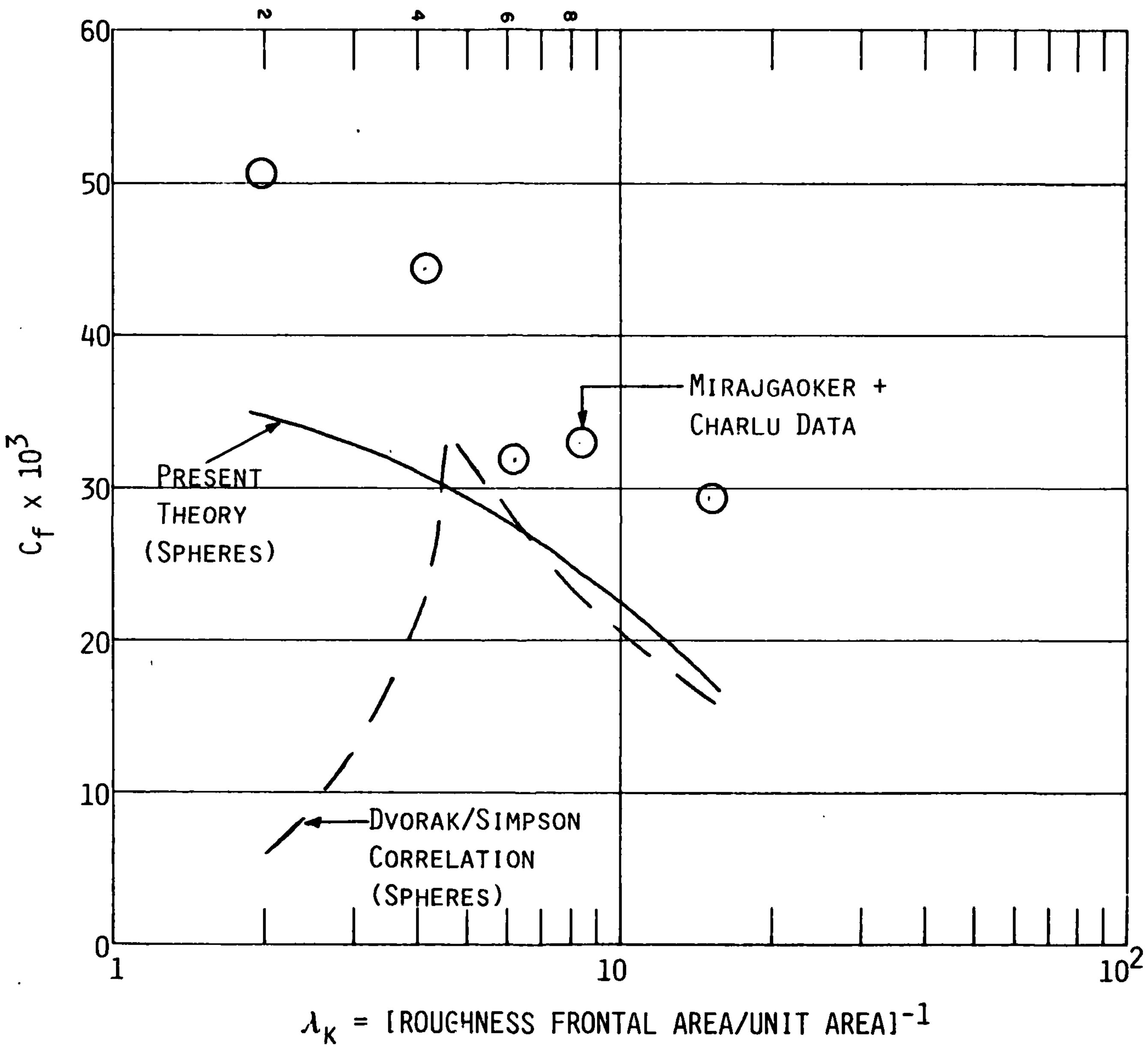

Fig. 8 Comparison of present model with the measurements of Miragaoker and Charlu[17] on stones at various spacings.

flume, and specified their stones as spheres. It is obvious that the theory significantly underpredicts the measured drag, as does Simpson's correlation.[26] The reasons for this discrepancy are unclear - perhaps free surface effects are important. However, no attempt has been made to investigate that possibility in this study.

5. COMPARISONS WITH COMPRESSIBLE ROUGHNESS DATA

The effect of surface roughness in compressible flow conditions remains poorly understood, perhaps largely because the available data base is rather fragmentary. In Ref. 33 we showed extensive comparisons with the PANT data on hemispherical nosetips at supersonic velocities, and we also demonstrated[34] satisfactory agreement with Keel's data[10] at $M_e = 4.8$. Here we shall present analyses of the recent measurements of Holden and Hill. Some preliminary comparisons were given in Ref. 34, but the diagnostic techniques and roughness characterizations have recently been extended and refined, permitting more definitive analyses at this time.

One interesting series of tests by Holden[9] were performed on 45° cones, at an edge Mach number of 1.8. These tests illustrate the importance of the method of applying grit to the model surface. Holden's most recent studies used a two-sided tape to apply the particles, whereas earlier methods used Krylon spray adhesive. Holden[9] kindly supplied us with profilometer traces of the surfaces prepared in each way from identical "4 mil" grit. Figure 9 shows the average elements derived by the method presented in Section 3. There is clearly a significant difference, with the two-sided tape yielding greater roughness height and density. Subsequent discussions with Holden led to the conclusion that various effects such as agglomeration can affect the bonding process. It is not sufficient to use the nominal grit or sand grain size as a measure of the roughness size.

In Fig. 10 we compare the present model with Holden's measured heat transfer data for the 4-mil tape mounted roughness. A significant error is seen in the absolute level of the smooth and rough wall computations. This error seems to be appreciable for cases with low values of T_w/T_e, at modest edge Mach numbers. At hypersonic speeds, viscous dissipation maintains high temperatures throughout most of the boundary layer and no such overprediction is found. This error, then, occurs for cases with extreme density or temperature variations across the boundary layer. Despite careful examination, we have not been able to remedy this discrepancy. Numerical accuracy does not seem to be the issue, and we can only speculate that existing turbulence closure approximations are inadequate in situations with large density gradients.

5299-9

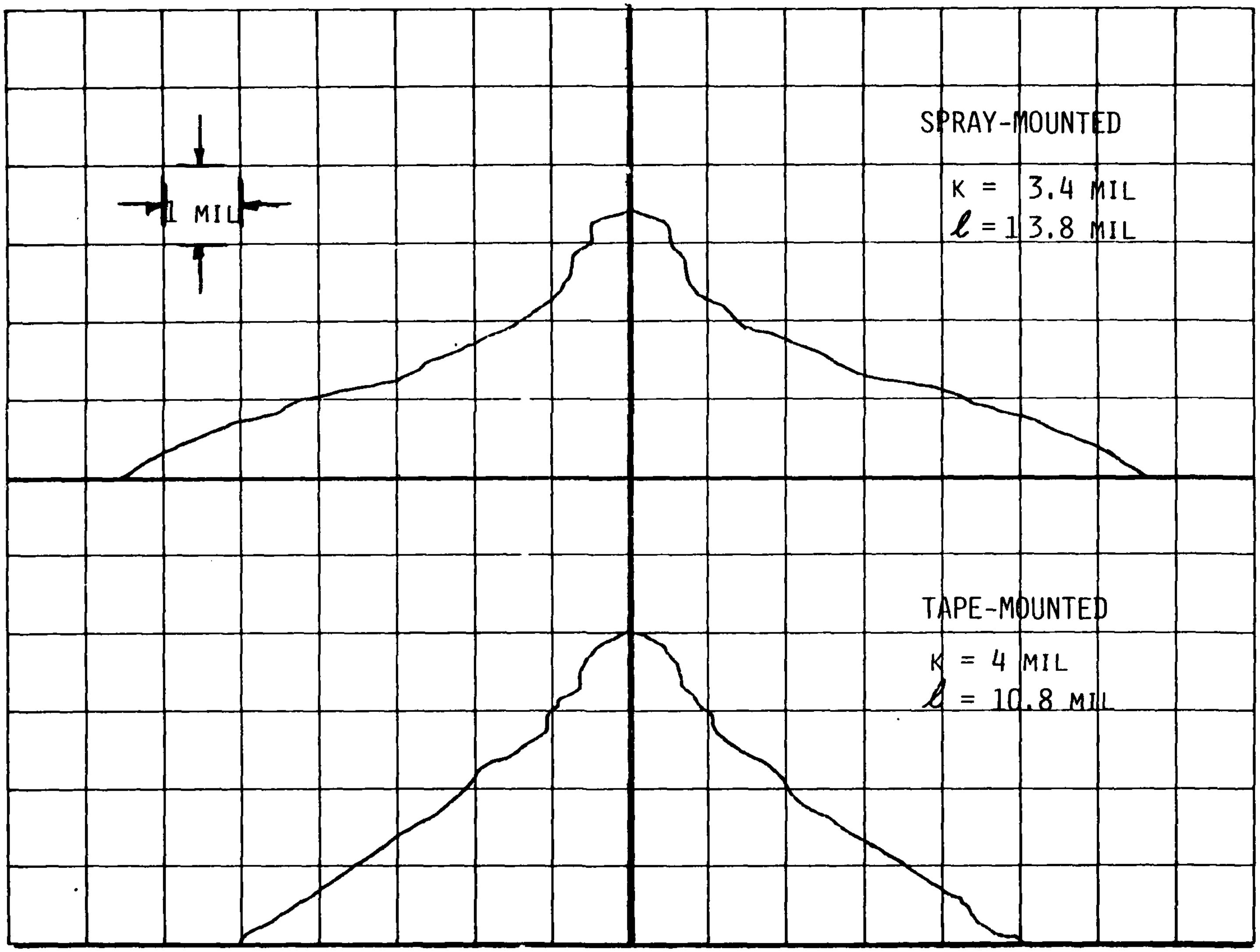

Fig. 9 Average roughness elements for Holden's[9] "4 mil" roughness, for two methods of application.

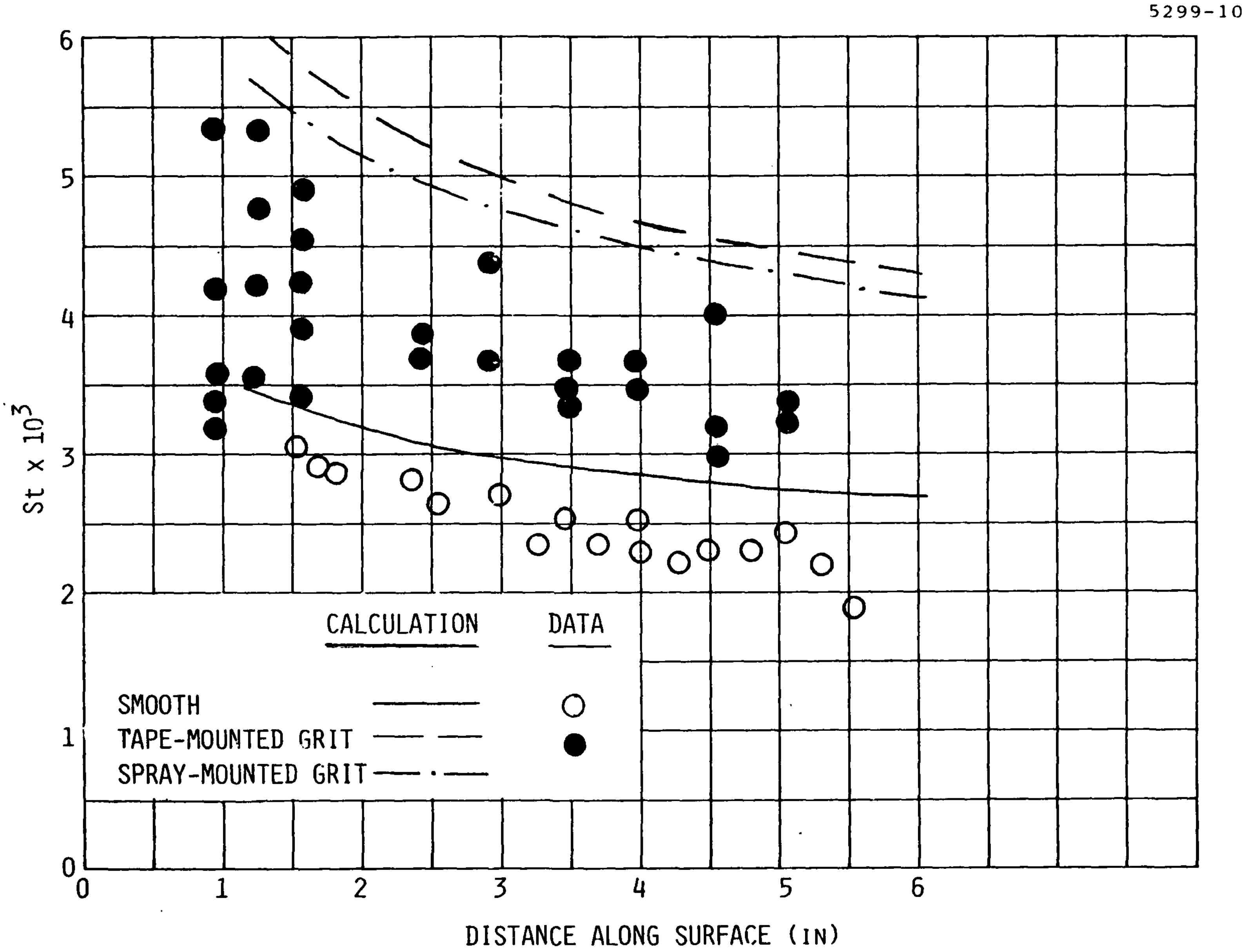

Fig. 10 Comparison of present model with Holden's heat transfer data on 4-mil tape model roughness.[9]

If one were to scale down the magnitude of the calculations, the extent of the predicted roughness augmentation would agree rather well with Holden's data for spray-mounted roughness. As also indicated, the model predicts less increase in heating for the Krylon-mounted roughness.

Two very significant experiments under similar hypersonic conditions were performed by Holden[13] and Hill,[12] on slender cones at $M_e = 8\text{-}10$. Holden used a single 10 mil (nominal) grit, and obtained measurements on the windward ray at angles of attack from 0° to 16°. To confirm earlier results with thin film gages, he used calorimeter heat transfer gages, in addition to skin friction gages. Hill used three different roughnesses, from nominal grit sizes of 11, 37 and 65 mils. Both experimenters provided us with profilometer traces, from which we derived the roughness parameters.

Figure 11 shows the roughness element specifications derived from the profilometer traces. Hill's method of application appears to result in elements that are more vertically aligned and more closely spaced on a relative basis. For three of these surfaces, the derived roughness height is close to the average grit diameter, but is very much less for Hill's "65 mil" grit. This finding emphasizes the need to perform careful characterizations of actual rough surfaces.

Figure 12 compares the present model with Holden's measurements. For the cases at angle of attack, we used an equivalent cone approximation to describe angle of attack effects, which might be less accurate at higher angles. Several trends are evident in Fig. 12. Roughness causes a greater increase in skin friction than in heat transfer. At $\alpha = 0^\circ$, Holden's results show little roughness effect at the larger downstream distances, whereas a modest effect is predicted. Greater increases, and better agreement between theory and data, are seen with increasing angle of attack.

The corresponding comparisons with Hill's heat transfer data are shown in Fig. 13. The predicted roughness heating is similar for all three of Hill's roughness. The 11 mil case is somewhat over-predicted, while the other two cases are underpredicted at greater downstream distances. Both theory and data indicate slightly higher heating values at 37 mils than at 65 mils. This behavior is compatible with the derived roughness characteristics shown in

5299-11

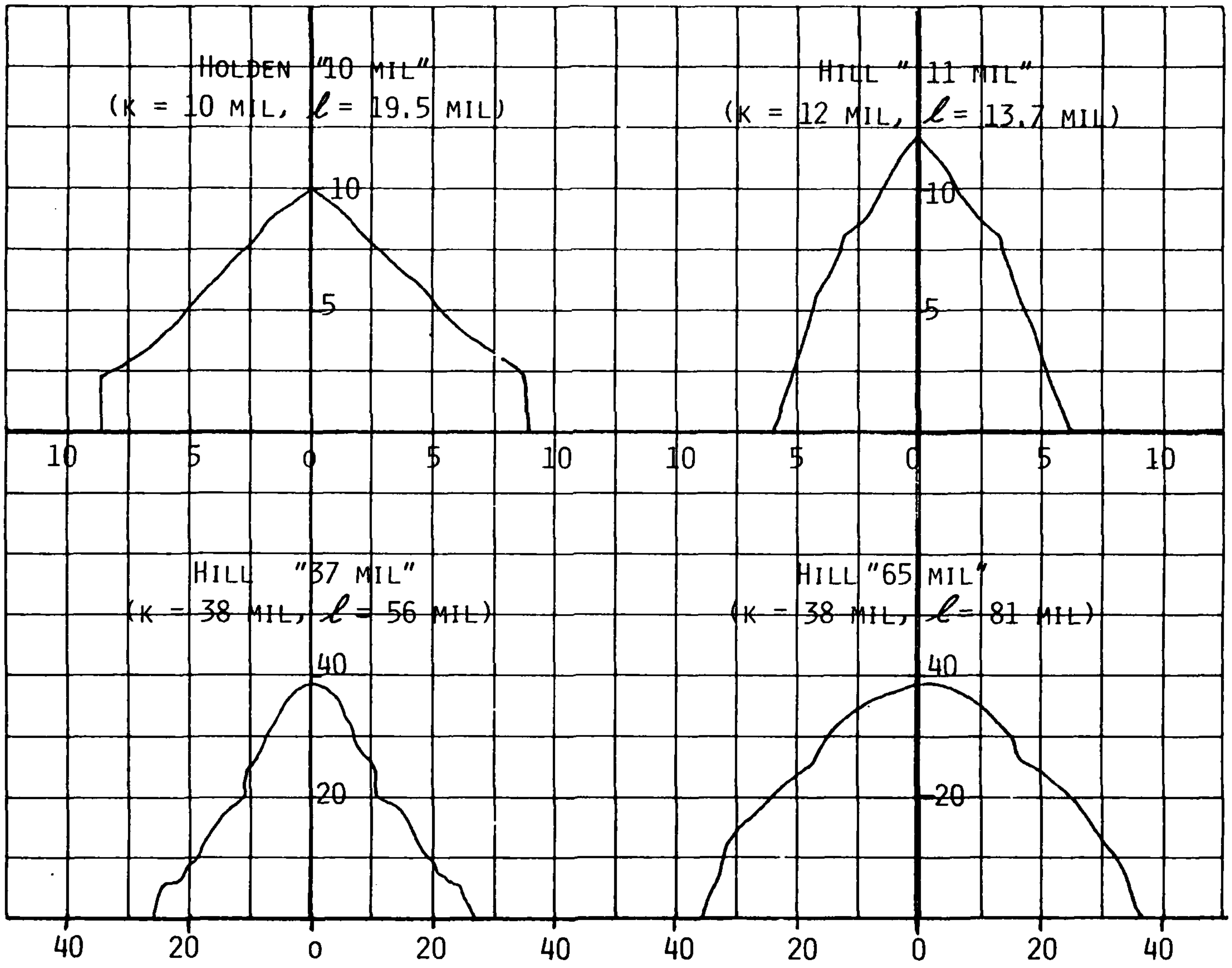

Fig. 11 Roughness descriptions derived from profilometer traces for the grit roughnesses of Hill[12] and Holden.[13]

5299-12

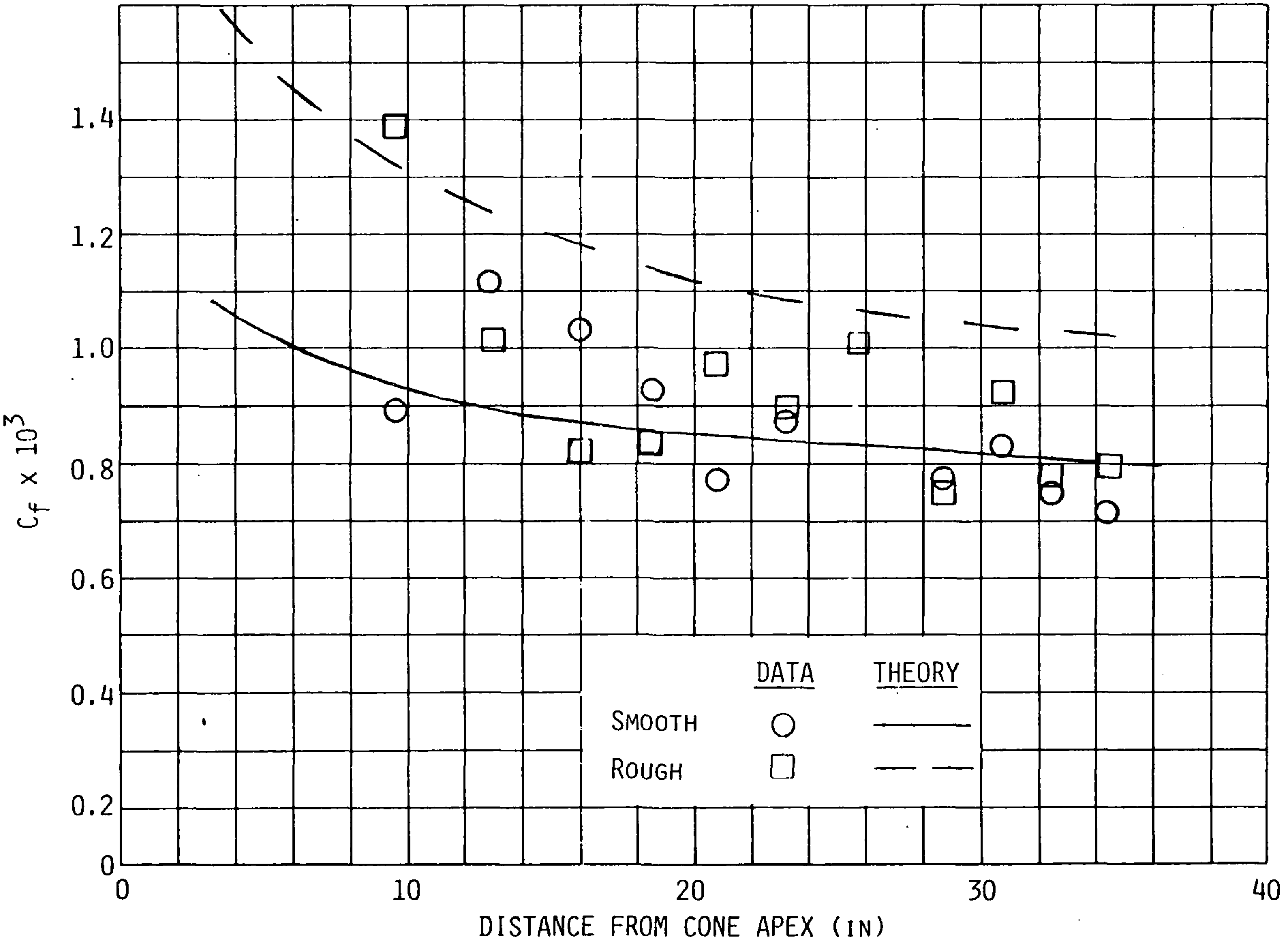

Fig. 12a Comparison of computed skin friction versus distance with Holden's data[13] on a 6° cone at $M_e = 9.4$, no angle of attack.

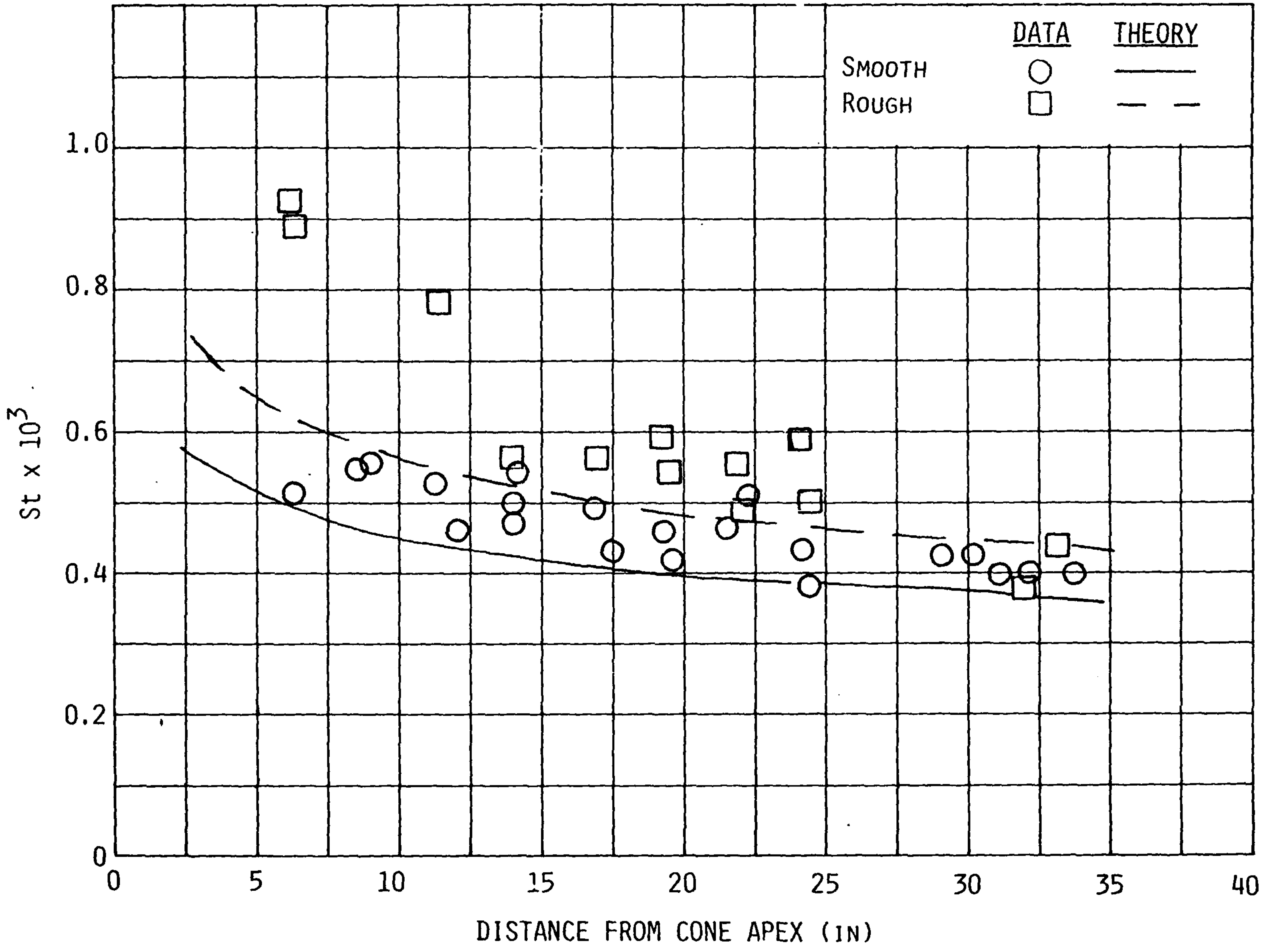

Fig. 12b Comparison of computed heat transfer versus distance with Holden's data[13] on a 6° cone at $M_e = 9.4$, no angle of attack.

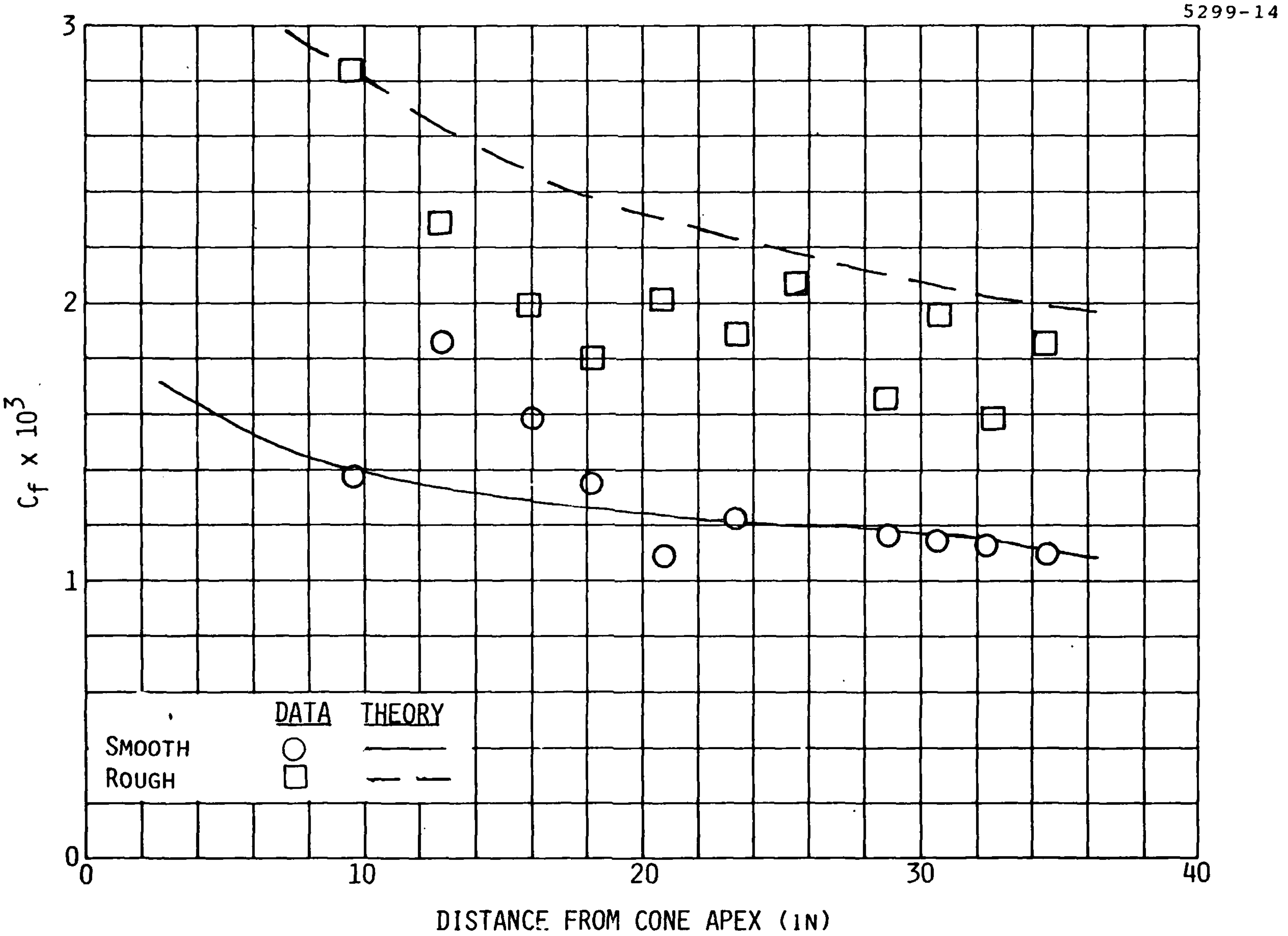

Fig. 12c Comparison of computed skin friction versus distance with Holden's data[13] on a 6° cone at $M_e = 6.3$ 8° angle of attack.

5299-15

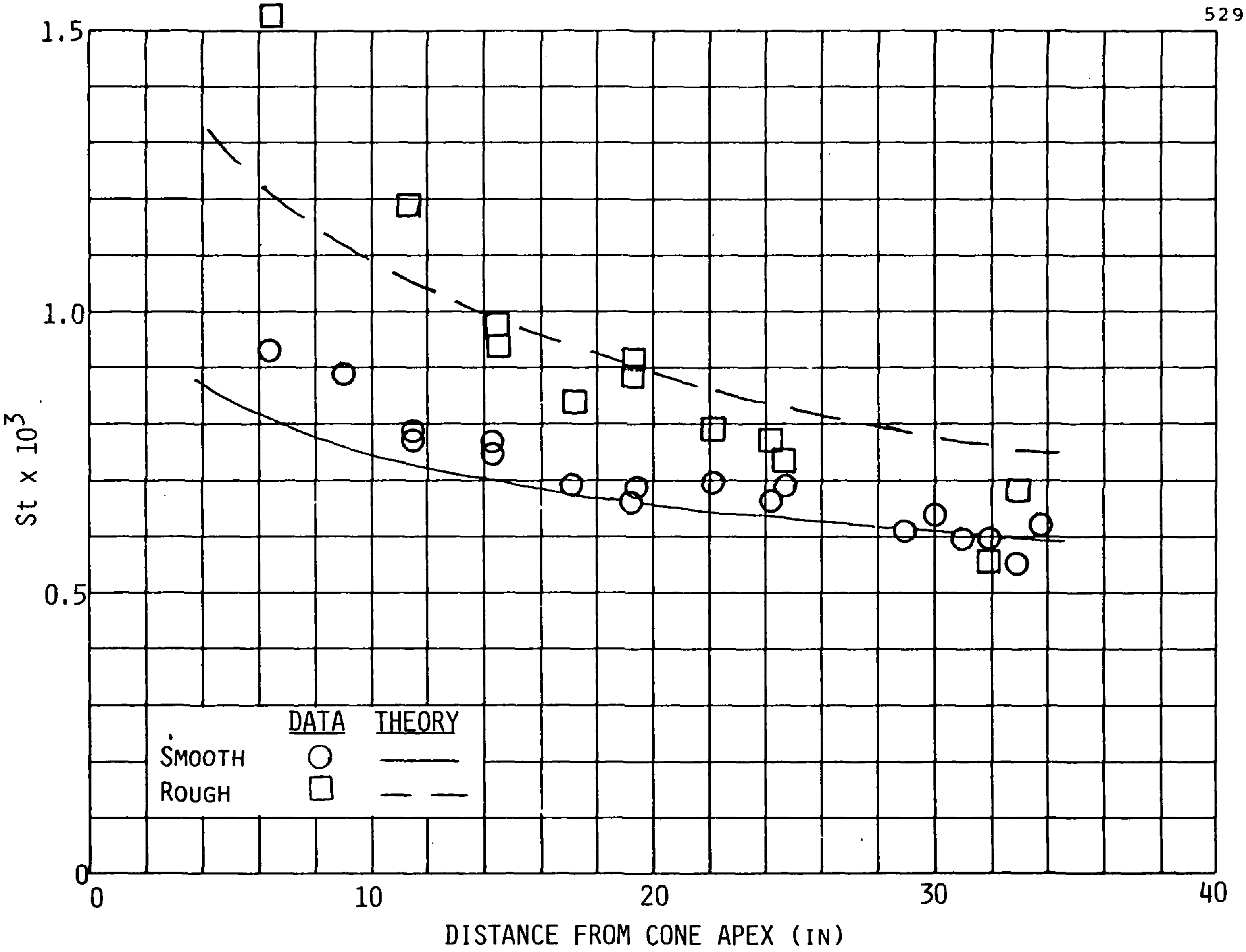

Fig. 12d Comparison of computed heat transfer versus distance with Holden's data[13] on a 6" cone at $M_e = 6.3$, 8° angle of attack.

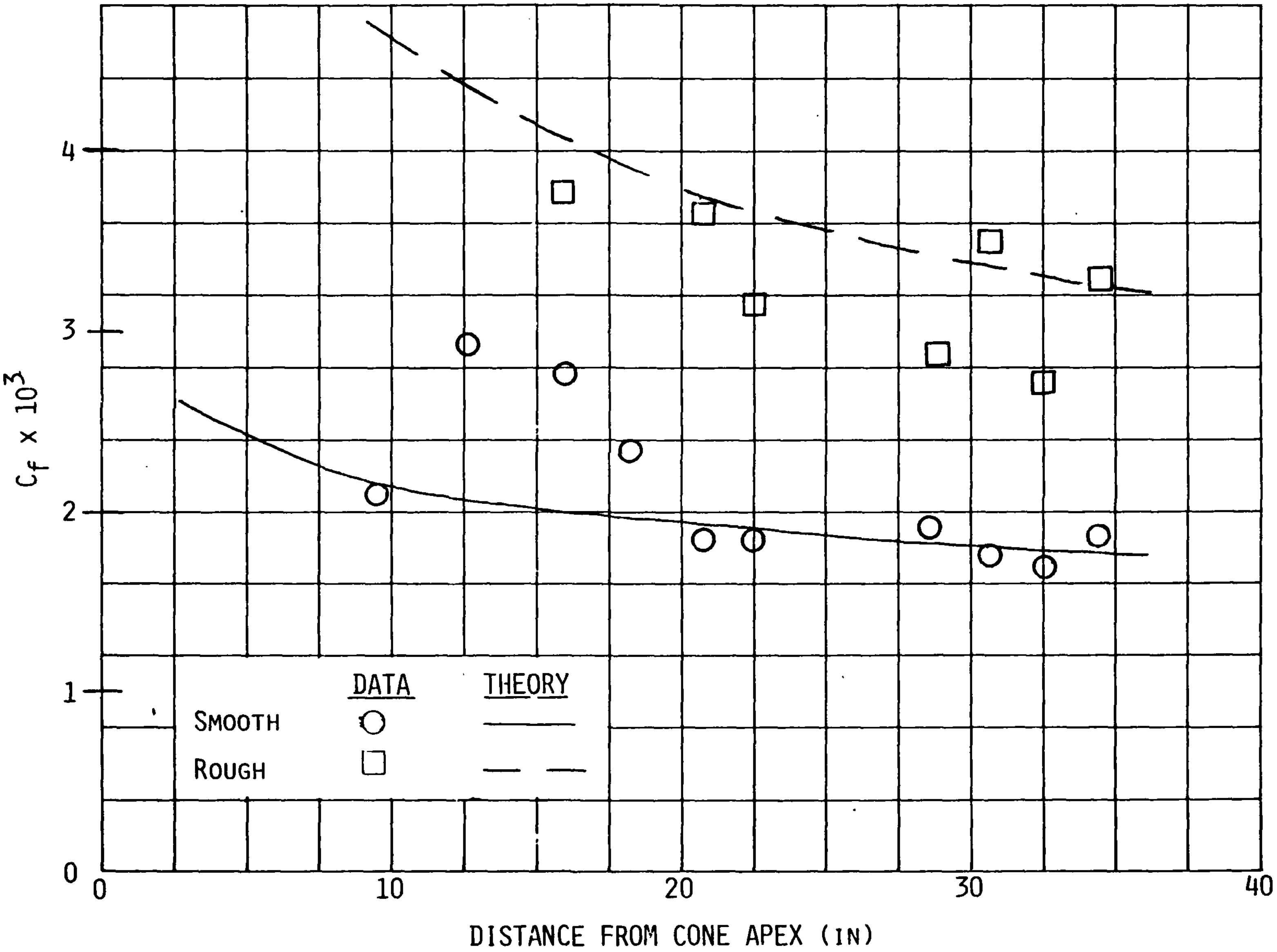

Fig. 12e Comparison of computed skin friction versus distance with Holden's data[13] on a 6° cone at $M_e = 4.4$, 16° angle of attack.

5299-17

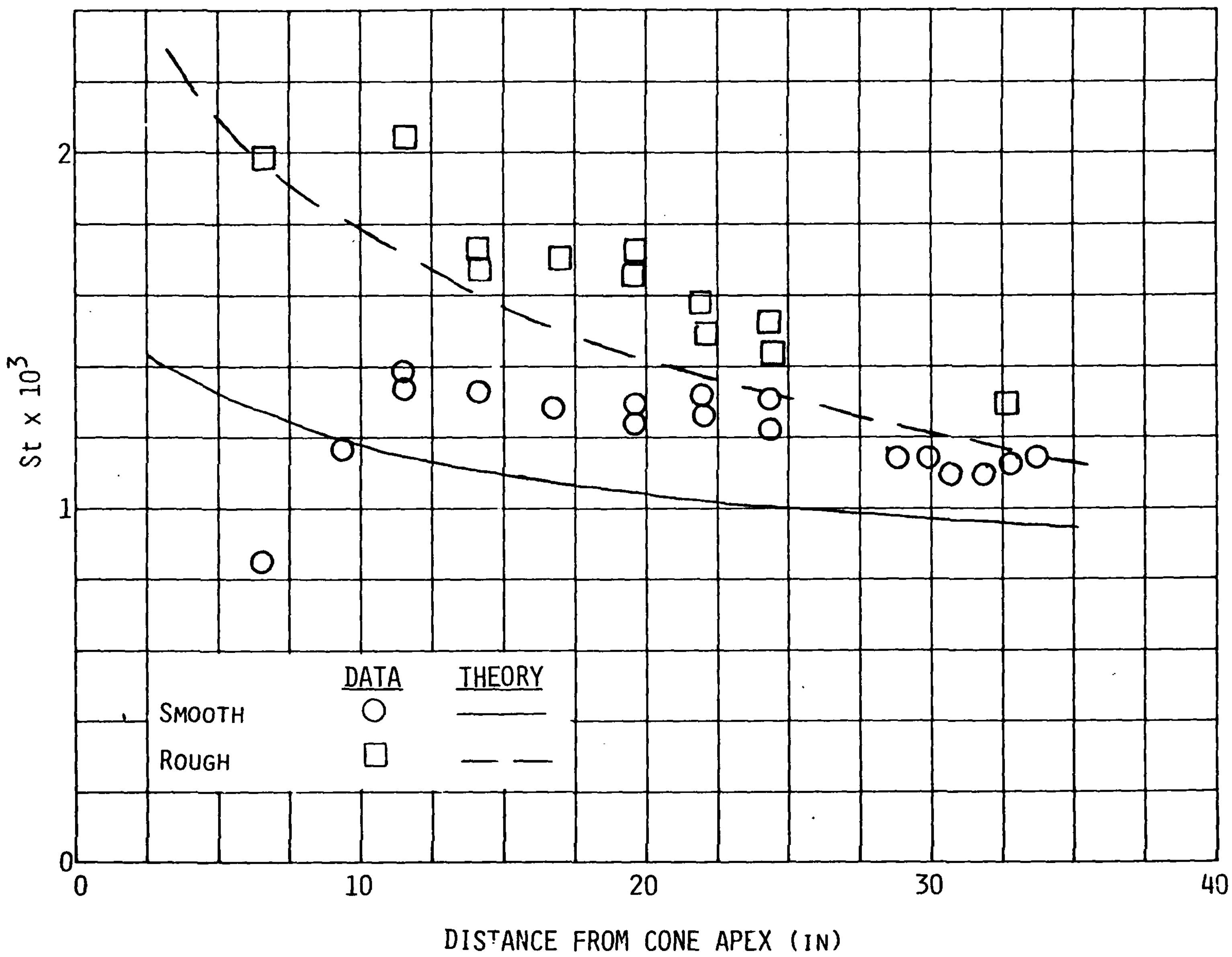

Fig. 12f Comparison of computed heat transfer versus distance with Holden's data[13] on a 6° cone at $M_e = 4.4$, 16° angle of attack.

5299-18

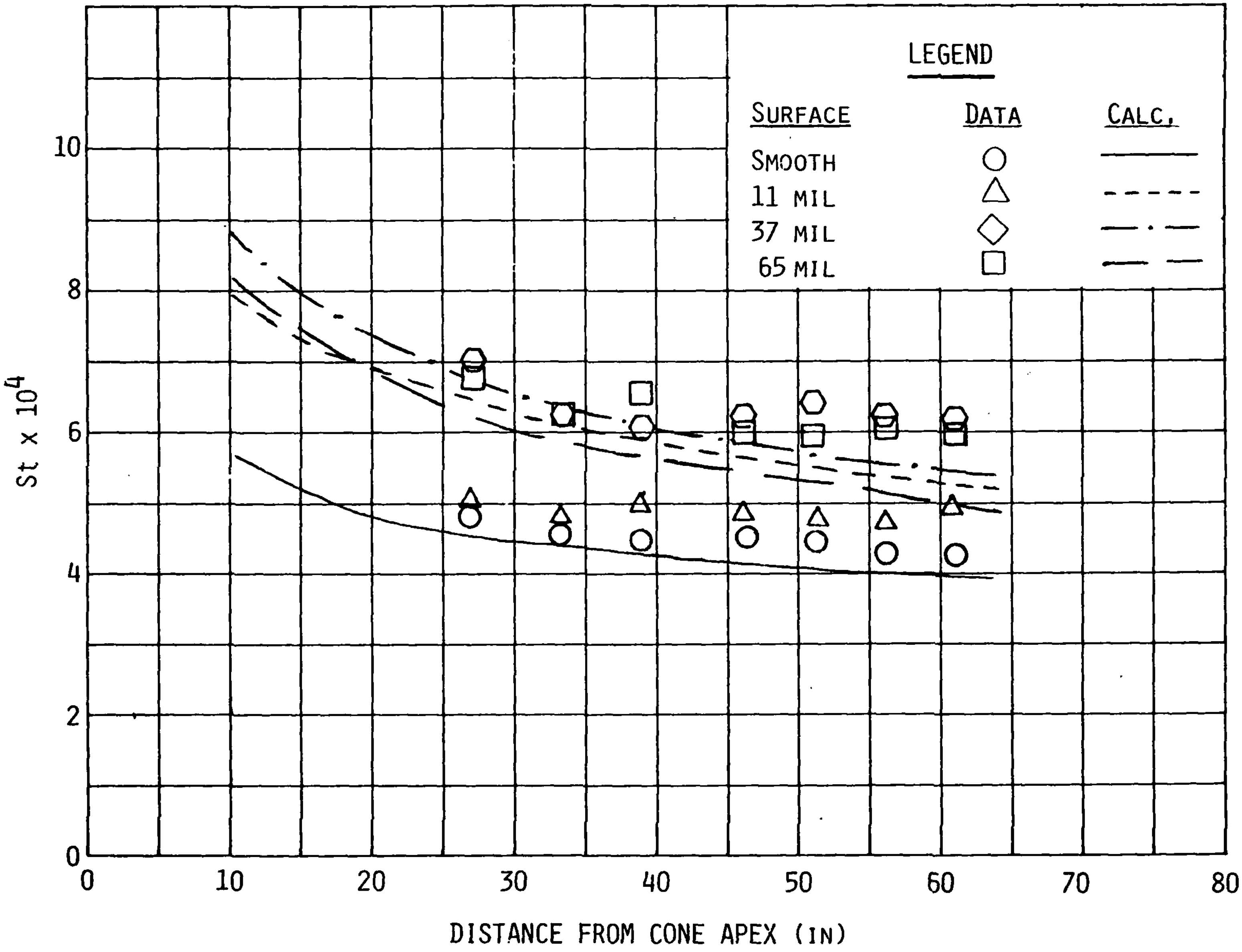

Fig. 13 Comparison of computed heat transfer versus distance with Hill's[12] data on 7° cones at $M_e = 8.1$.

Fig. 11, which showed the same height but greater spacing for the 65 mil grit. One puzzling aspect of Hill's data is the tendency of the rough wall heating rates to be essentially independent of distance. If anything, we would expect the rough wall measurements to decay at a greater rate than the smooth wall data, since k/θ decreases with increasing distance.

The 10 mil data of Holden at 0^{o} angle of attack and the 11 mil data of Hill are significant, in that very little effect of roughness is evident in either case. The present theory and most existing correlations predict at least a moderate effect. It is suggested below that relatively modest roughness Reynolds numbers are responsible for this behavior. The quantity k^{+} is 50-70 for either case, but is much larger for Holden's cases at nonzero angles of attack and for Hill's cases at larger roughness. Such k^{+} values are only slightly below the fully-rough requirement of $k^{+} = 70$ for incompressible flows, However, careful examination of our computer results indicates that the transition values should increase with increasing Mach number, to be discussed more extensively below.

6. ROUGHNESS SCALING LAW

While the model presented above yields good general agreement with the available data, it is not particularly useful for engineering purposes. The computational cost of running the computer code is modest. However, it is impractical to expect other users to become familiar with the program, which involves finite difference solution of many simultaneous, stiff partial differential equations. What is needed is an algebraic recipe that can be readily understood and applied to practical problems. Our computer model can be useful in developing such an engineering method in two ways: 1) numerical solutions can be examined to determine the dominant physical processes and 2) the code can be exercised to generate a base of numerical data covering the range of input parameters far more thoroughly than do the available experiments.

The key to developing scaling laws for roughness effects lies in the computed mean velocity profiles. For the vast majority of cases considered, the mean velocity is quite uniform over much of the range $y < k$. An example is shown in Fig. 14, from our solution for Schlichting's closely packed spherical segments. Near the top of the elements the velocity profile increases and blends into the log region, and the velocity must decrease towards zero as $y \to 0$. But the velocity is remarkably constant for most of the region $y < k$. The exceptional cases, in which a range of uniform velocity is not evident, generally involve such short or sparse roughnesses that the smooth wall profile is hardly altered.

It must be admitted that this velocity behavior was not anticipated in our model development. Physically, for $y < k$ the turbulence is simply diffusing toward the base of the wall and dissipating. Perhaps an approximate model could be developed, for example by a three-layer approach (the constant velocity region, the log region, and the outer region). There is little experimental evidence to confirm or deny the predicted behavior, since it is generally not feasible to measure flow properties between roughness elements. Chen and Roberson[15] show a profile that increases by only 10-20% in the range $0.2 < y/k < 1$, for hemispheres at an average spacing of 4.5 diameters. This velocity profile behavior is apparently well known in the study of turbulence

5299-19

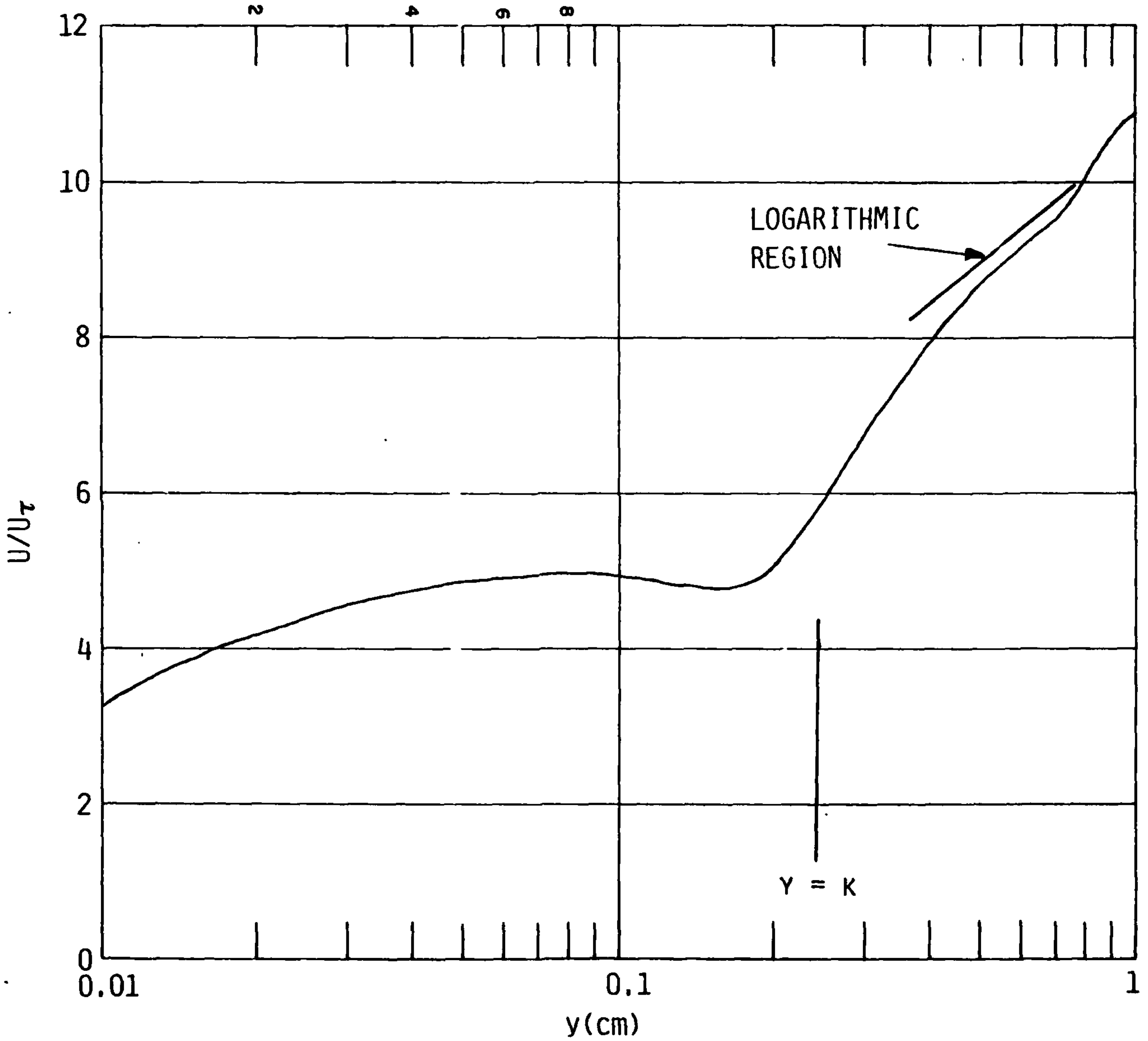

Fig. 14 Computed mean velocity profile for a typical case (closely packed spherical segments).

in plant canopies, and Raupach and Thom[37] quote two measured wind profiles in plant canopies (a pine forest and a maize field) that are quite similar to that of Fig. 14.

The wall shear is given by

$$C_f = C_{f_{sm}} + \int_o^k \frac{\rho U^2}{\rho_e U_e^2} \quad C_D f(y) \frac{D(y)}{\ell^2} \, dy \ , \tag{14}$$

(the blockage factor f(y), defined in Eq. (10) , enters through the stream function). Now let us approximate U as a constant $U = U_R$. For compressible cases, ρ will be related to U, and hence is also constant $\rho = \rho_R$. The blockage factor generally varies slowly with height and will be approximated by its value at k/2. Since the integral of D(y) is simply the frontal area of the roughness element, Eq. (14) reduces to

$$C_f = C_{f_{sm}} + \frac{\rho_R}{\rho_e} \frac{U_R^2}{U_e^2} C_D f\left(\frac{k}{2}\right) \lambda_k^{-1} \quad , \tag{15}$$

which is the basis for deriving the appropriate scaling laws.

6.1 Incompressible Fully-Rough Flow

Equation (15) may be contrasted to Eq. (2)

$$\left(\frac{2}{C_f}\right)^{1/2} = \left(\frac{2}{C_{f_{sm}}}\right)^{1/2} - \frac{\Delta U_1}{U_\tau} \quad . \tag{2}$$

For sand grain roughness, the velocity shift in the fully rough regime is

$$\frac{\Delta U_1}{U_\tau} = 5.6 \log k_s^+ - 3 \quad . \tag{3}$$

The smooth wall skin friction involves the Reynolds number based on some measure of the width of turbulent layer. We shall select the momentum thickness θ as the appropriate thickness.* To a very good approximation

$$\left(\frac{2}{C_{f_{sm}}}\right)^{1/2} = 5.6 \log Re_\theta + C \ , \tag{16}$$

where C depends on flow geometry and pressure gradient. Putting Eqs. (3) and (16) into Eq. (2) shows that the skin friction is solely a function of k/θ for fully rough conditions

$$\begin{aligned} \left(\frac{2}{C_f}\right)^{1/2} - 5.6 \log \left(\frac{2}{C_f}\right)^{1/2} \\ = 3 + C - 5.6 \log k_s/\theta \end{aligned} \tag{17}$$

We have run our computer code over a wide range of parameters such as roughness shape and spacing. We first confirmed that C_f is a function only of k/θ, within the available numerical accuracy. Figure 15 shows an example of the computed behavior, for hemispherical roughness elements at three relative spacings; k^+ varies substantially. The spread of the computed points for each spacing is indicative of the numerical accuracy. The curves represent Eq. (17), with k_s chosen to match the computed values at $k/\theta = 1$.

---

*The boundary layer thickness is most analogous to the radius of a pipe or half-height of a channel. However, boundary layer models compute δ inaccurately (in our case) or not at all (in most integral methods). The displacement thickness δ^* is also not a good measure for compressible situations, for which it becomes quite sensitive to the density ratio across the boundary layer.

5299-20

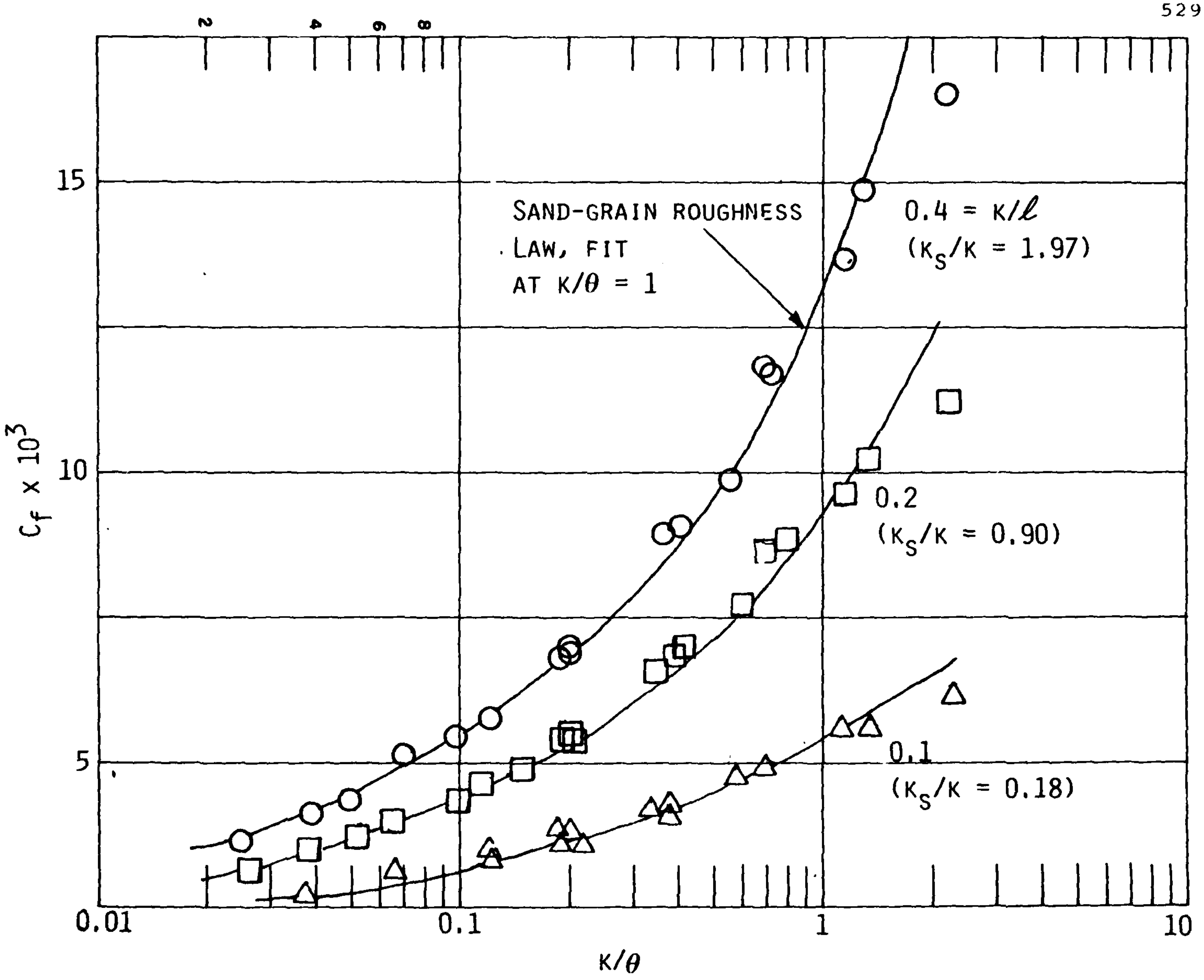

Fig. 15 Computed skin friction versus k/θ for three spacings, along with classical variation predicted with sand-grain roughness law.

Equations (15) and (17) represent two alternate views of roughness effects. Equation (17) explicitly shows the dependence on k_s/θ, but contains no information on roughness character; Eq. (15) is useful for displaying roughness character. If C_f is to depend only on k/θ and roughness character, then U_R must depend on the same quantities and must also depend weakly on Re_θ in such a fashion as to cancel the weak dependence of ${C_f}_{sm}$ on Re_θ. In practice, we have correlated U_R from computed values of C_f at any Re_θ and k^+ in the fully rough regime, specifying ${C_f}_{sm}$ as the flat plate value at $Re_\theta = 10^5$. So long as the same value of ${C_f}_{sm}$ is retained, the resulting correlations for U_R can be used at any Re_θ or k^+ in the fully rough regime.

We have developed a numerical data base for roughness character effects from boundary layer runs with a variety of roughness shapes and spacings. The shapes considered were hemispheres, spheres, cylinders (diameter = height), 30° (half-angle) cones, 45° cones, and truncated 30° cones (top diam = base diam/2). Spacing was generally varied from $k/\ell = 0.1$ to as closely packed as numerically feasible. From the computed values of C_f, along with $C_D = 0.6$, $\rho_R/\rho_e = 1$, ${C_f}_{sm} = 1.81 \times 10^{-3}$ for our flat plate solution at $Re_\theta = 10^5$, and the appropriate values of $f(k/2)$ and λ_k, we then solved Eq. (15) for U_R/U_e. An example of the derived values is shown in Fig. 16 for hemispheres. The straight lines are drawn as an aid to the eye; U_R/U_e cannot be precisely linear in log k/θ and still have consistency between Eqs. (15) and (17.)

The other shapes investigated yield plots quite similar to that of Fig. 16. In fact, if one were to approximate the numerically derived values of U_R with straight lines as indicated in Fig. 16, the height and slope of the lines are almost solely a function of λ_k and quite insensitive to element shape. Such a correlation for U_R as a function of k/θ and λ_k could then be used in Eq. (15) as a useful engineering tool. However, it is more precise and more compatible with existing methods to correlate U_R vs. λ_k at a fixed value of k/θ (such as unity) and then use Eqs. (15) and (17) to derive the effective sand grain roughness. In Fig. 17 we show the derived values of U_R at $k/\theta = 1$ for all of the shapes considered. A modest shape dependence may be

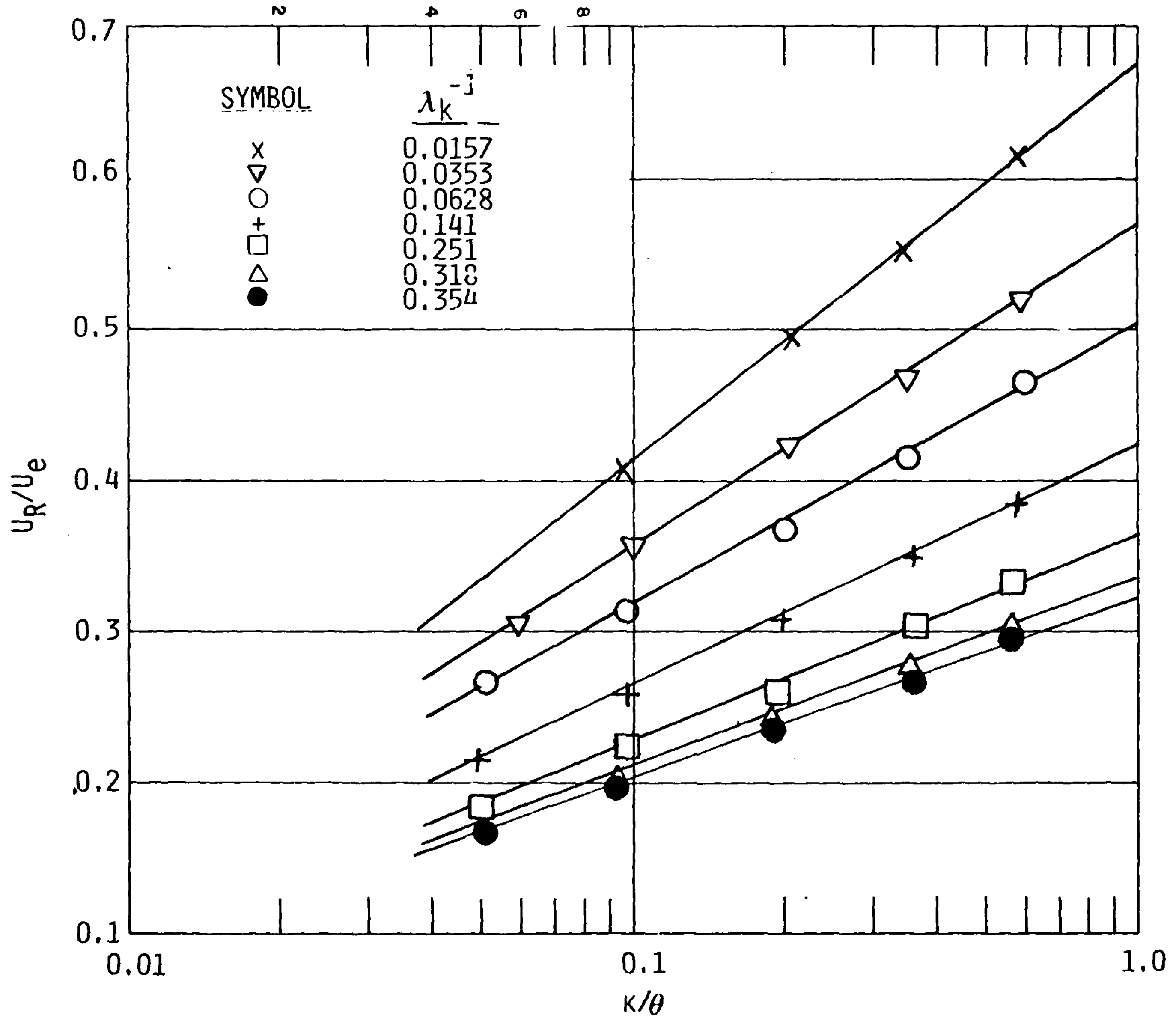

Fig. 16 Derived values of roughness velocity versus k/θ, for hemispherical roughness at various spacings.

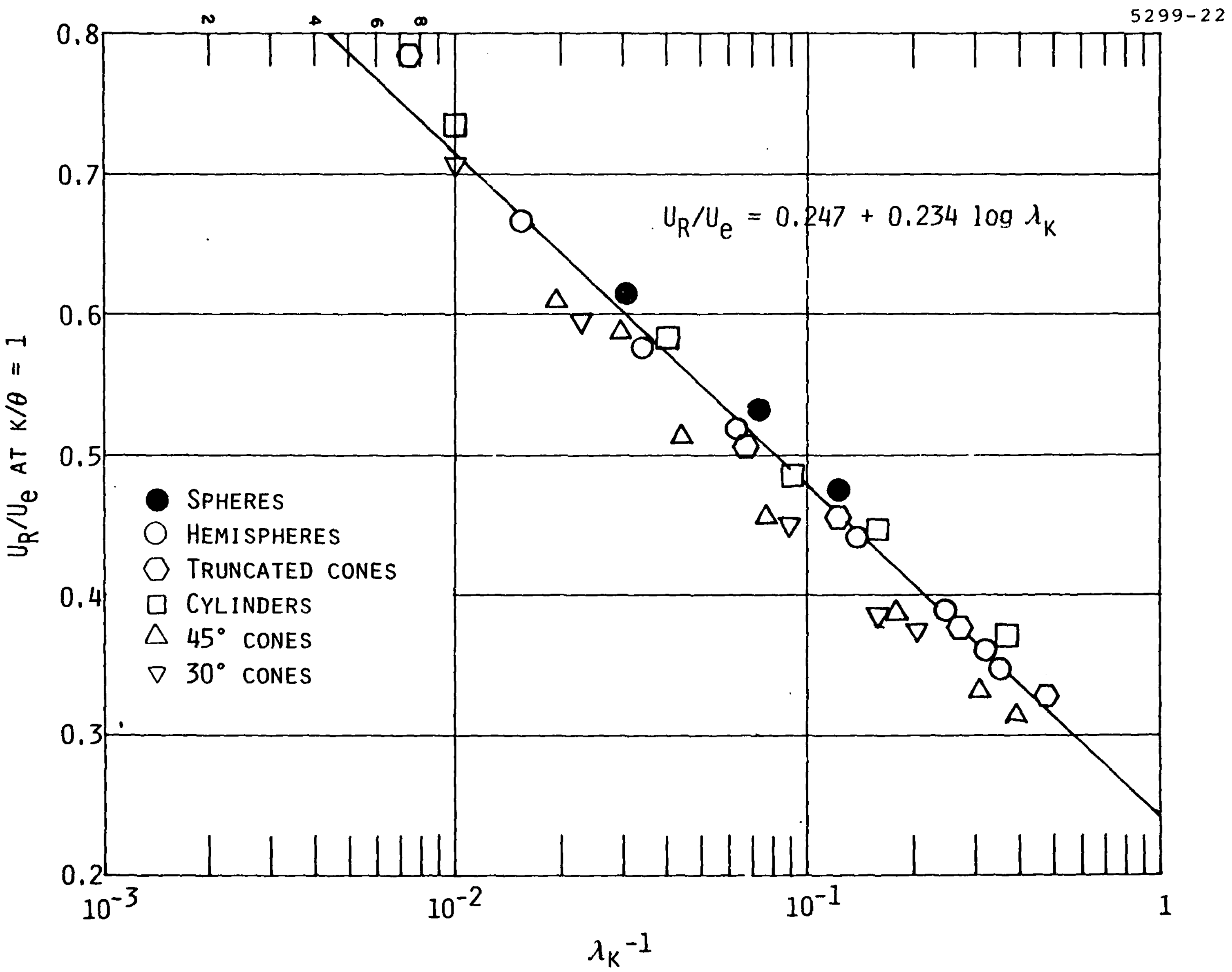

Fig. 17 Correlation of roughness velocity at k/θ = 1.

detected, with conical elements tending to fall below the more blunt shapes. The correlation suggested in the figure best fits the more blunt shapes, which may be more representative of actual surface roughnesses; also, our theory tends to underpredict the roughness effect observed for cones by Schlichting.[14]

If one inserts the indicated correlation

$$\frac{U_R}{U_e} = 0.247 + 0.234 \log \lambda_k \qquad (18)$$

along with $C_{f_{sm}} = 1.81 \times 10^{-3}$, $C = 5.24$, and $C_D = 0.6$ into the above equations, the following equations result for the ratio of sand grain to actual roughness height,

$$C_{f_i}^* = 1.81 \times 10^{-3} + 0.6(0.247 + 0.234 \log \lambda_k)^2 \, f\left(\frac{k}{2}\right) \frac{1}{\lambda_k} \qquad (19a)$$

$$5.6 \log k_s/k = 8.50 - \left(\frac{2}{C_{f_i}^*}\right)^{1/2} + 5.6 \log\left(\frac{2}{C_{f_i}^*}\right) \qquad (19b)$$

Figure 18 compares the value of k_s/k predicted by Eq. (19) with the actual observed values, for a number of experiments involving roughness character. Two sets of data are seriously underpredicted by the present correlation (as well as by the computer model - cf. Figs. 6 and 8): Schlichting's short angles[14] (baffles) and the stones of Mirajgoaker and Charlu.[17] We have no explanation for these discrepancies. The tall rods of Seginer et al.[22] and Thom[21] are rather substantially underpredicted.

For comparison, Fig. 19 shows a similar comparison for the correlation of Simpson,[26] a refinement of Dvorak's correlation.[24] The general degree of correlation is comparable to that of the present result. The short angles of Schlichting and stones of Mirajgoaher and Charlu are again underpredicted; the rods of Seginer are handled decently, but those of Thom could not even be plotted on the figure. It is most important to note that the Simpson (and Dvorak) correlation is not accurate for closely packed roughness elements.

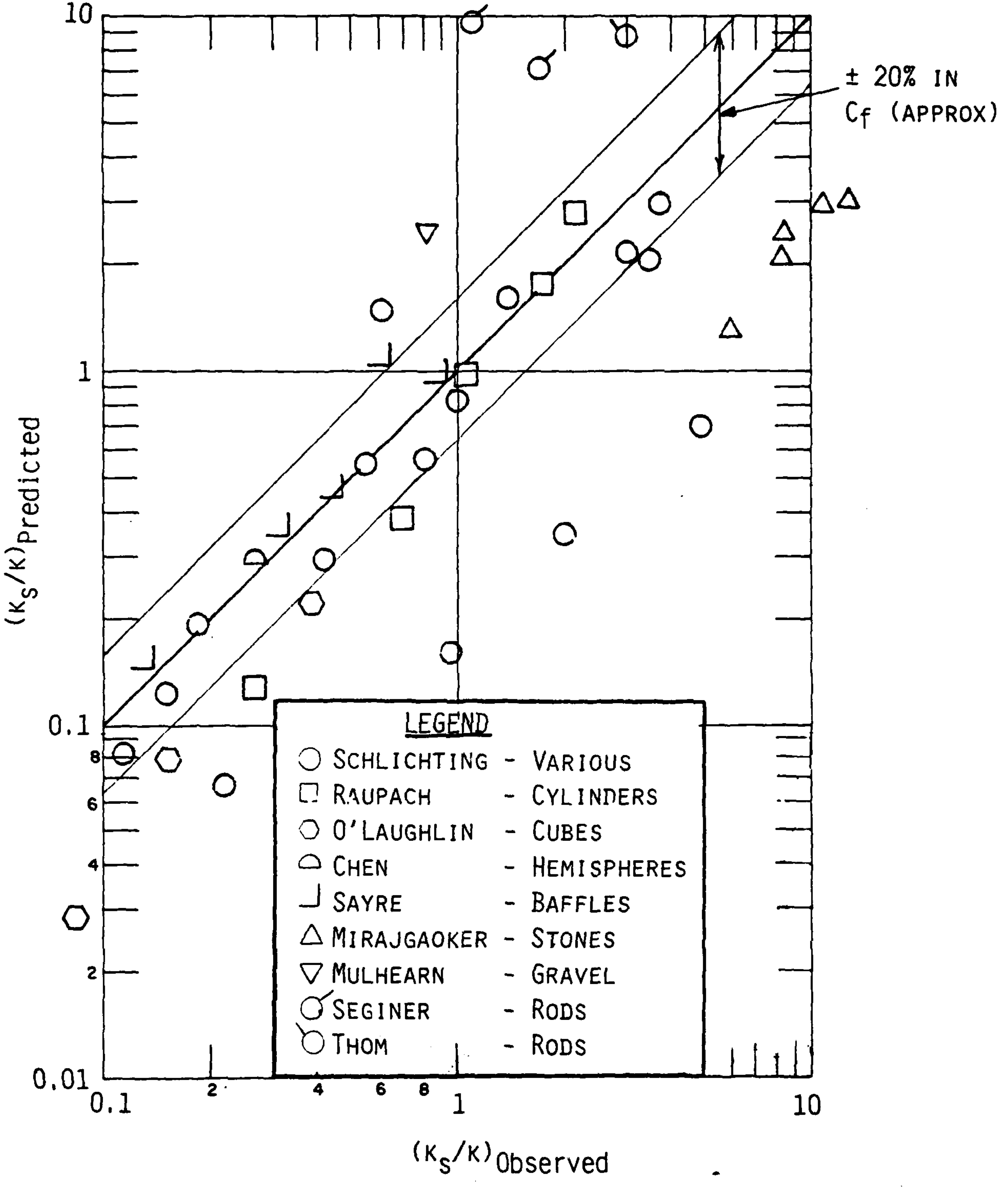

Fig. 18 Comparison of predicted versus actual roughness for present result.

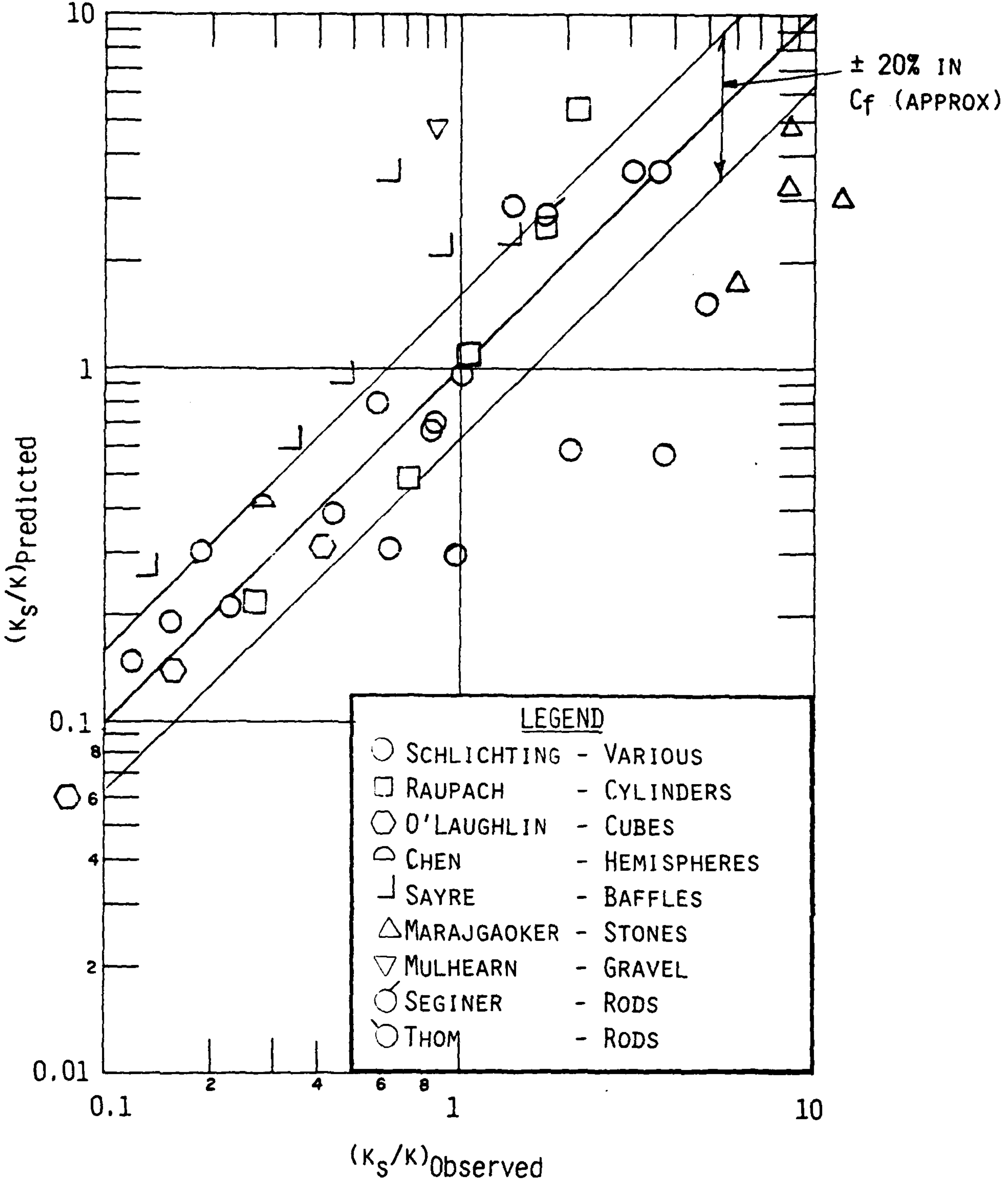

Fig. 19 Comparison of predicted versus actual roughness for Simpson's correlation.

The points for Schlichting's closely packed spheres, spheres with $\ell/D = 1.5$, and closely packed spherical segments all fall outside the indicated ± 20% error band in Fig. 19. Most of the available experimental data on roughness character have been obtained with relatively sparse roughness patterns. The Simpson/Dvorak correlations are fine tuned to the data base, but do not have the benefit of sufficient distributed roughness data at greater roughness densities. Use of the straight line segment with positive slope in Fig. 1 leads to the poor results cited and Simpson questioned the validity of that portion of the correlation for 3-D roughness. Hence, for relatively closely-packed roughness (say $\ell/k < 1.5$), which corresponds to most surfaces of practical interest, the correlation derived here should be the more reliable.

6.2 Compressible Flows-Fully Rough

Compressibility effects generally reduce friction on both smooth and rough walls. Smooth wall friction coefficients are generally computed from "transformation functions," F_θ and F_c. As reviewed in Ref. 29, an equivalent incompressible coefficient is computed at the effective Reynolds number $F_\theta \cdot Re_\theta$, and is then divided by F_c to obtain the compressible coefficient:

$$C_{f_{sm}} = \frac{1}{F_c} C_{f_{i,s_m}} (F_\theta \cdot Re_\theta) \qquad (20)$$

As noted above, Dvorak[24,25] used Eq. (2) to obtain a rough wall incompressible friction coefficient, evaluating $C_{f_{sm}}$ at $F_\theta \cdot Re_\theta$ and $\Delta U_1/U_\tau$ at the actual value of k^+; he then divides by F_c according to Eq. (20). Note that F_θ plays a very small role - F_θ is usually near unity and $C_{f_{sm}}$ is insensitive to Reynolds number. If F_θ plays no role, then this procedure guarantees that the percentage increase of friction is independent of compressibility, at fixed k/θ. Our model, however, predicts a rather different result - that the relative effect of roughness decreases with increasing Mach number.

In the present model, one obvious effect of compressibility is through the density. At high Mach numbers, viscous dissipation causes high temperatures within the boundary layer. Because roughness reduces velocities within the boundary layer, even higher temperatures can be expected. To estimate the roughness density, we evaluated the relation between total enthalpy and velocity in the output from a large number of computer runs at edge Mach numbers between 0 and 10. A linear relationship was found to be quite accurate

$$\frac{H-h_w}{H_e-h_w} = \frac{U}{U_e} \tag{21}$$

as it is with nearly any turbulent situation. Then, with perfect gas relations it follows easily that

$$\frac{T_R}{T_e} = \left(\frac{\rho_R}{\rho_e}\right)^{-1} = \frac{T_w}{T_e} + \left(1 + \frac{\gamma-1}{2} M_e^2 - \frac{T_w}{T_e}\right)\frac{U_R}{U_e} - \frac{\gamma-1}{2} M_e^2 \frac{U_R^2}{U_e^2} \tag{22}$$

Figure 20 compares this equation with the values of ρ_R (at $y = k/2$) and U_R from several runs of the computer model. Except at $M_e = 10$, $T_w/T_e = 0.74$, where Eq. (22) is perhaps 20% high, the equation provides a simple and accurate representation of the density.

The roughness density term can obviously significantly reduce the magnitude of the friction predicted by Eq. (15). This reduction is similar to, but not precisely the same as, that obtained by dividing an incompressible value by F_c. To a good approximation (as in the Sommer-Short method[29]), F_c is given by the reference temperature

$$F_c = \frac{T_{ref}}{T_e} = 0.55 + 0.45 \frac{T_w}{T_e} + 0.035 M_e^2 . \tag{23}$$

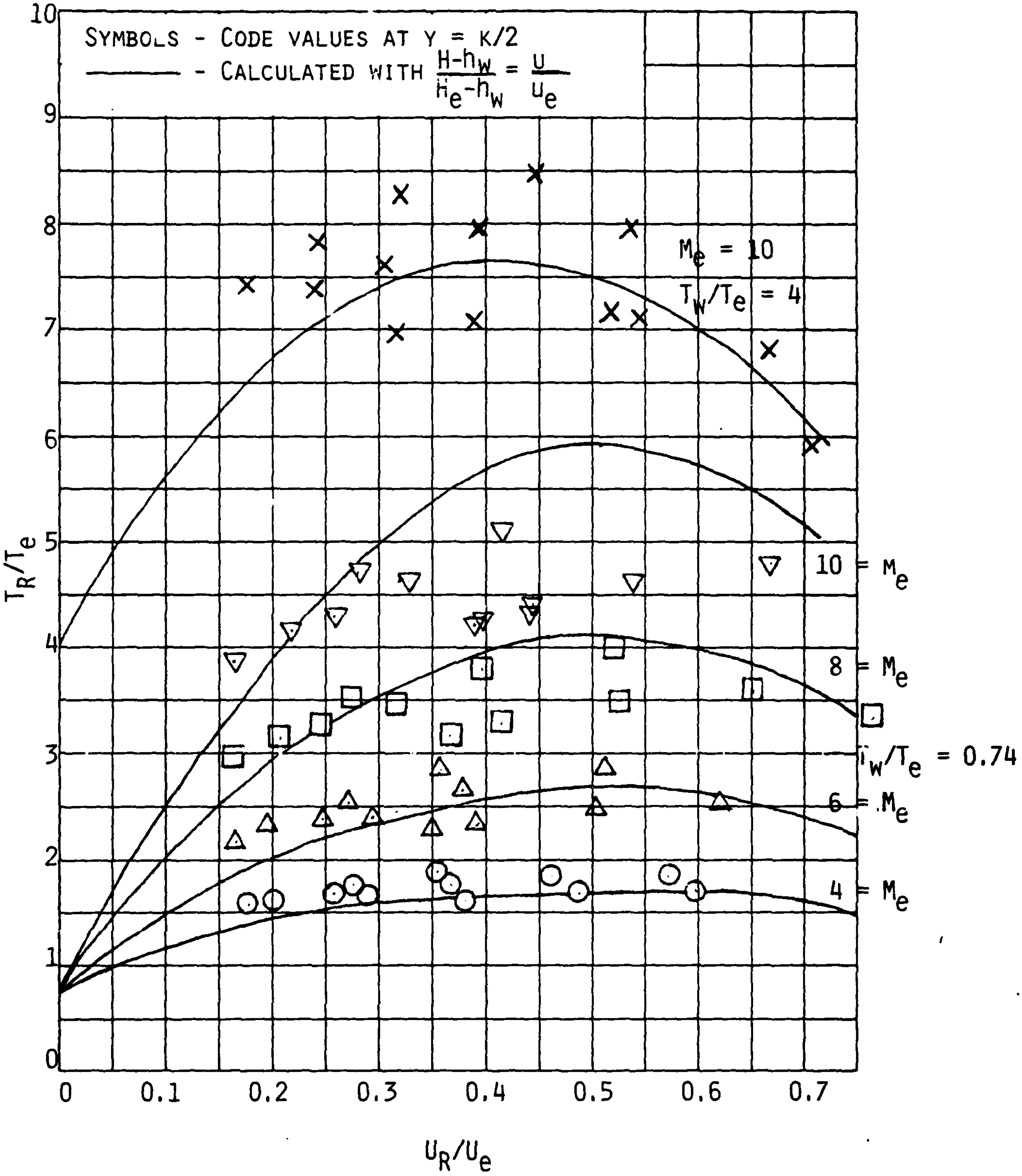

Fig. 20 Roughness temperature or density scaling law versus values from computer model.

The value of T_{ref} tends to be somewhat below the values of T_R given by Eq. (22) or Fig. 20 - for $T_w/T_e = 0.74$ they agree at $U_R/U_e = 0.23$; at $T_w/T_e = 4$, they agree at $U_R/U_e = 0.12$. However, the computer model indicates an additional effect, in that U_R is affected by compressibility.

A careful examination of the values of U_R/U_e derived from our computer solutions, over a wide range of Mach numbers and/or wall temperature ratios, indicates that the roughness velocity scales with $\rho_R \lambda_k / \rho_e$, as indicated in Fig. 21. Note that most of the scatter about the incompressible correlation results from cases where the wall temperature ratio was varied; our computer code has inherent inaccuracies for cases with T_w/T_e very small or large, even for smooth walls. Otherwise, Fig. 21 shows a rather solid correlation for the effect of compressibility on U_R. Note, however, that this correlation

$$\frac{U_R}{U_e} = 0.247 + 0.234 \log\left(\frac{\rho_R}{\rho_e}\right) \lambda_k \tag{24}$$

is a transcendental equation for U_R, since ρ_R depends on U_R through Eq. (22). But, ρ_R is typically insensitive to U_R, and one can iterate to a solution very quickly.

Computation of the compressible skin friction requires first the compressible coefficient at $k/\theta = 1$, analogous to the incompressible value given by Eq. (19a):

$$C_f^* = \frac{1.81 \times 10^{-3}}{F_c} + 0.6 \frac{\rho_R}{\rho_e} \left[0.247 + 0.234 \log \left(\frac{\rho_R}{\rho_e} \lambda_k \right) \right]^2 f\left(\frac{k}{2}\right) \frac{1}{\lambda_k} \tag{25}$$

The friction coefficient at general values of k/θ is then given by

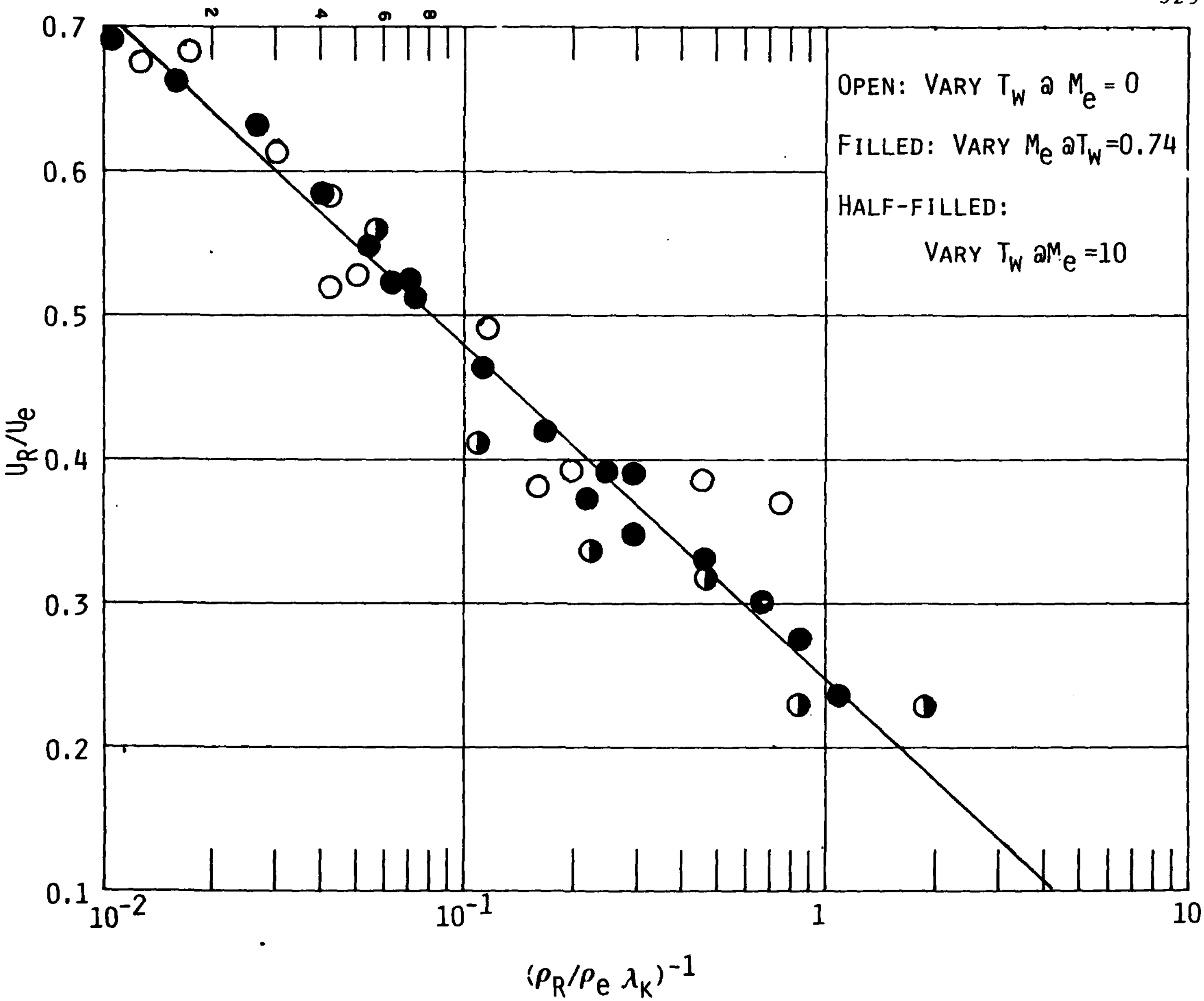

Fig. 21 Correlation of roughness velocity at $k/\theta = 1$ for compressible cases.

$$\left(\frac{2}{C_f}\right)^{1/2} - 5.6\sqrt{F_c}\,\log\left(\frac{2}{C_f}\right)^{1/2} = \left(\frac{2}{C_f{}^*}\right)^{1/2}$$

$$- 5.6\sqrt{F_c}\,\log\left(\frac{2}{C_f{}^*}\right)^{1/2} - 5.6\sqrt{F_c}\,\log\frac{k}{\theta}\ . \tag{26}$$

Again, we have a transcendental equation, but one that is easily solved iteratively.

If one prefers to express the answer in terms of an equivalent sand-grain roughness (from incompressible data or Eqs. (19)), then there must be an upward shift in the velocity

$$\left(\frac{2}{C_f}\right)^{1/2} = \left(\frac{2}{C_{f_{sm}}}\right)^{1/2} - \sqrt{F_c}\,\frac{\Delta U_1}{U_\tau}\,(k^+) + \frac{\Delta U_3}{U_\tau}\ . \tag{27}$$

Here, $C_{f_{sm}}$ is the actual compressible smooth wall value and $\Delta U_1/U_\tau$ is calculated from the low speed relation (Eq. 3) using the actual wall conditions for k^+. The "compressibility shift" depends on roughness character and compressibility conditions (M_e, T_w/T_e):

$$\frac{\Delta U_3}{U_\tau} = \left(\frac{2}{C_f{}^*}\right)^{1/2} - 5.6\sqrt{F_c}\,\log\left(\frac{2}{C_f{}^*}\right)^{1/2}$$

$$- 8.5\sqrt{F_c} + 5.6\sqrt{F_c}\,\log\left(\sqrt{\frac{\rho_e}{\rho_w}}\ \frac{\nu_e}{\nu_w}\right), \tag{28}$$

where $C_f{}^*$ comes from Eq. (25).

This shift can be substantial - for example, for hemispheres at $k/\ell = 0.4$, $M_e = 10$, $T_w/T_e = 0.74$, the value is 14.3.

6.3 Rough/Smooth Transition

With Nikuradse's sand grain roughness, the transition between rough and smooth wall behavior occurs in the range $5 < k_s^+ < 70$. It is questionable whether the sand grain behavior could be applied to cases with varying roughness character or Mach number. Dvorak[24] presents an interpolation method for the transitional regime, but there is very little supporting data for 3-D roughness. We have investigated this issue with our computer model, recognizing the likely limitations of the theory. The form drag assumption is basically a high Reynolds number concept. Viscous drag on the elements is simply lumped into the underlying smooth wall friction, and there is no reason to believe that our computer model accurately describes drag on roughness elements at lower Reynolds numbers. Interference between neighboring elements also becomes more important with decreasing Reynolds numbers. However, the results are certainly interesting.

Figure 22 shows the values of Nikuradse's quantity B (-3 is replaced by 5.5-B in Eq. (3)) derived from our computer calculations for hemispherical roughness at three spacings. The derived values depart from the fully rough behavior ($B = 8.5$) at approximately the same value of k_s^+ for all three spacings. The more dense patterns show a transitional behavior similar to that observed by Nikuradse, at least within the accuracy of our calculations. However, the solutions for wide spacing show a completely different behavior.

The transitional behavior is even more complex for supersonic flows. Our solutions consistently indicate that minimum k^+ value for fully rough behavior increases with increasing Mach number. In Fig. 23 we show curve fits through the derived values of B with increasing edge Mach number, for hemispheres at $k/\ell = 0.4$ (the scatter of the computer data is substantial, but the trends are clear). Two effects are apparently involved here. First, the smooth wall solution tends to shift to increasing values of k^+ with increasing Mach number, as the compressibility term $\Delta U_3/U_\tau$ increases. Second, as discussed above with regard to fully rough behavior, the effective temperature in

5299-27

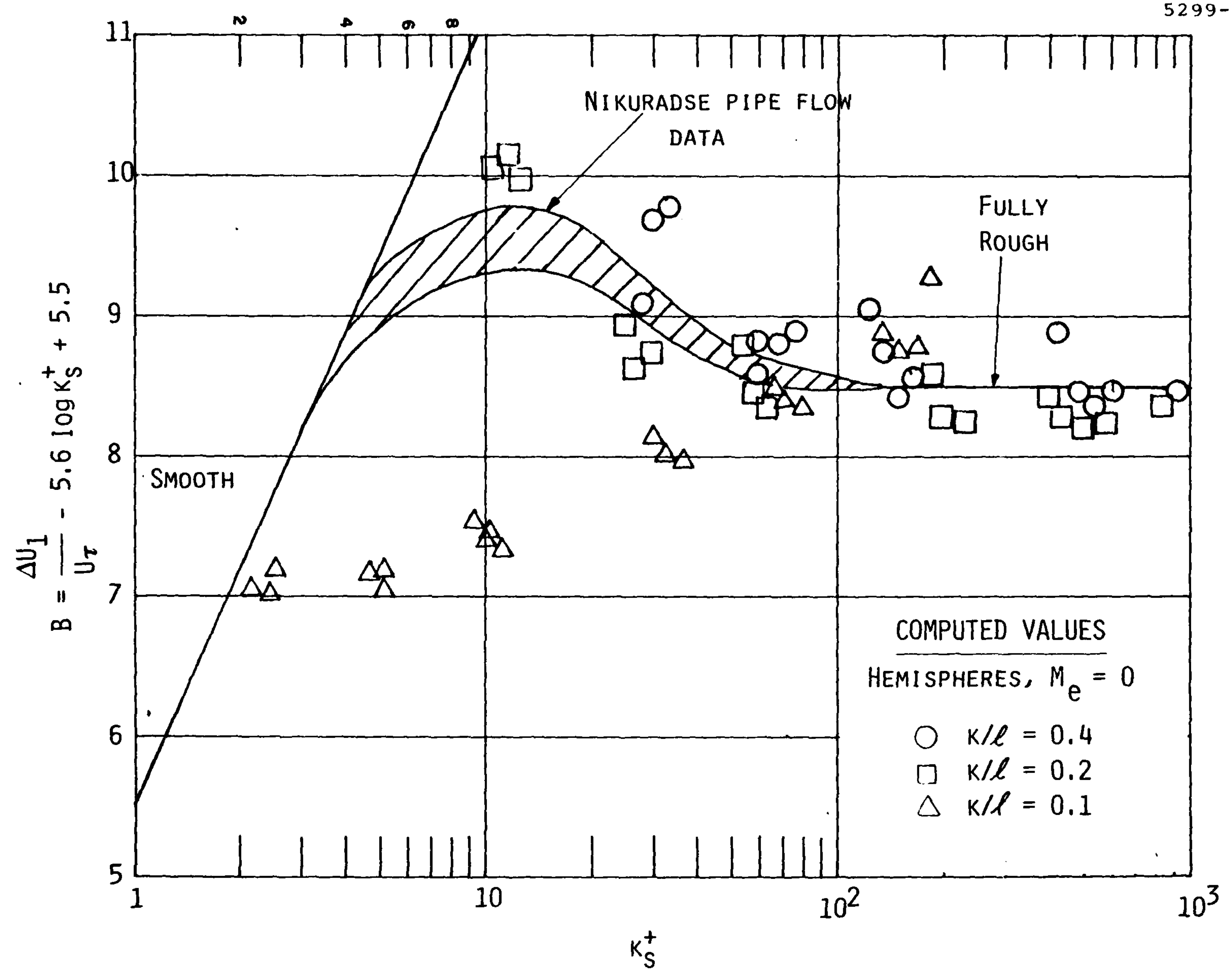

Fig. 22 Computed rough-smooth transition behavior in low speed flow.

5299-28

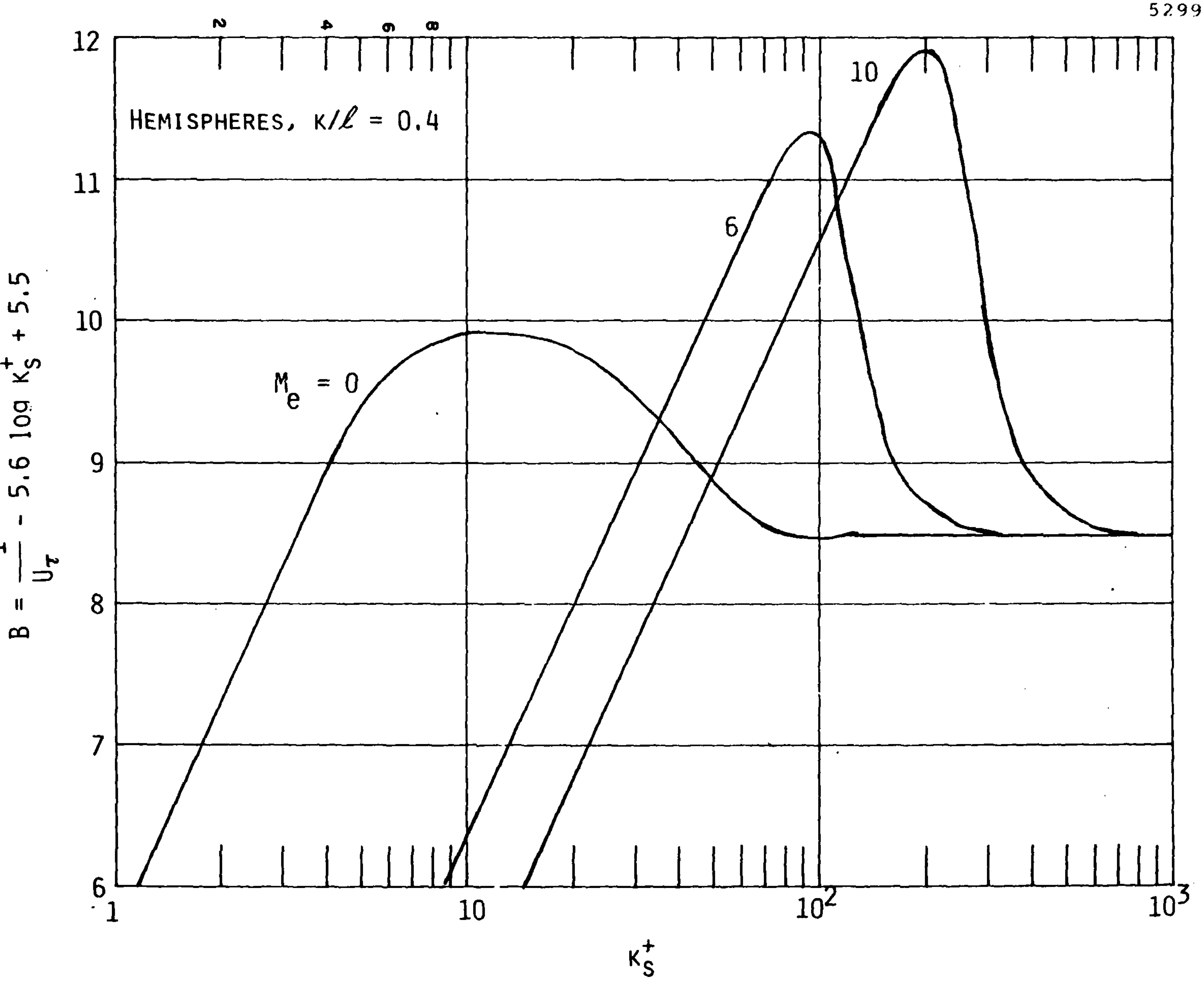

Fig. 23 Computed rough-smooth transition behavior versus Mach number.

the vicinity of the roughness elements should reflect the substantial viscous dissipation that occurs at high edge Mach numbers. Even for relatively low values of k^+, according to our solutions, the fluid properties at $y = k/2$ or $y = k$ will differ significantly from wall conditions, upon which k^+ is based. For example, for the Mach 10 case shown in Fig. 23 at $k_s{}^+ = 300$, where the solution shows definite departure from the fully rough regime, the temperature at $y = k/2$ is about 3.6 T_e or 4.8 T_w. With properties based on this temperature, rather than T_w, the resulting value of $k_s{}^+$ would be reduced by a factor of 6, bringing it into reasonable alignment with the low speed curve.

Figure 24 shows the computed velocity shift for conditions corresponding to Holden's experiments at zero angle of attack, plotted against k^+ ($k = 10$ mil, $k_s = 22$ mil from Eq. (19b)). As indicated, the test conditions correspond to $k^+ = 50\text{-}70$, where the solution definitely departs from the fully rough solution. The computer model yields a C_f value about 35% below the fully rough value for the same k/θ. The fact that Holden's measurements are virtually indistinguishable from smooth wall values suggests that the true departure from fully rough behavior is even greater than predicted at $k^+ = 50\text{-}70$. The conditions for Hill's 11 mil roughness are very much the same. Thus, we conclude that a combination of compressibility and transitional (smooth/rough) effects combine to cause the minimal augmentation observed in both cases. However, it would be foolhardy to attempt to derive a detailed description of the rough/smooth transition zone from the present model, and a much better data base is clearly needed.

6.4 Rough Wall Prandtl Number

It is commonly observed that roughness causes a smaller augmentation of heat transfer than of skin friction. In terms of the present model, this results from the fact that there is no thermal analogy to form drag. We previously[33,34] noted that all components of the fluctuating velocity are increased proportionally by roughness, while the fluctuating temperature is essentially unchanged from the smooth wall value. This reasoning suggests that the augmentation in the heat flux ($-\overline{v'h'}$) is the square root of that of the friction ($-\overline{u'v'}$)

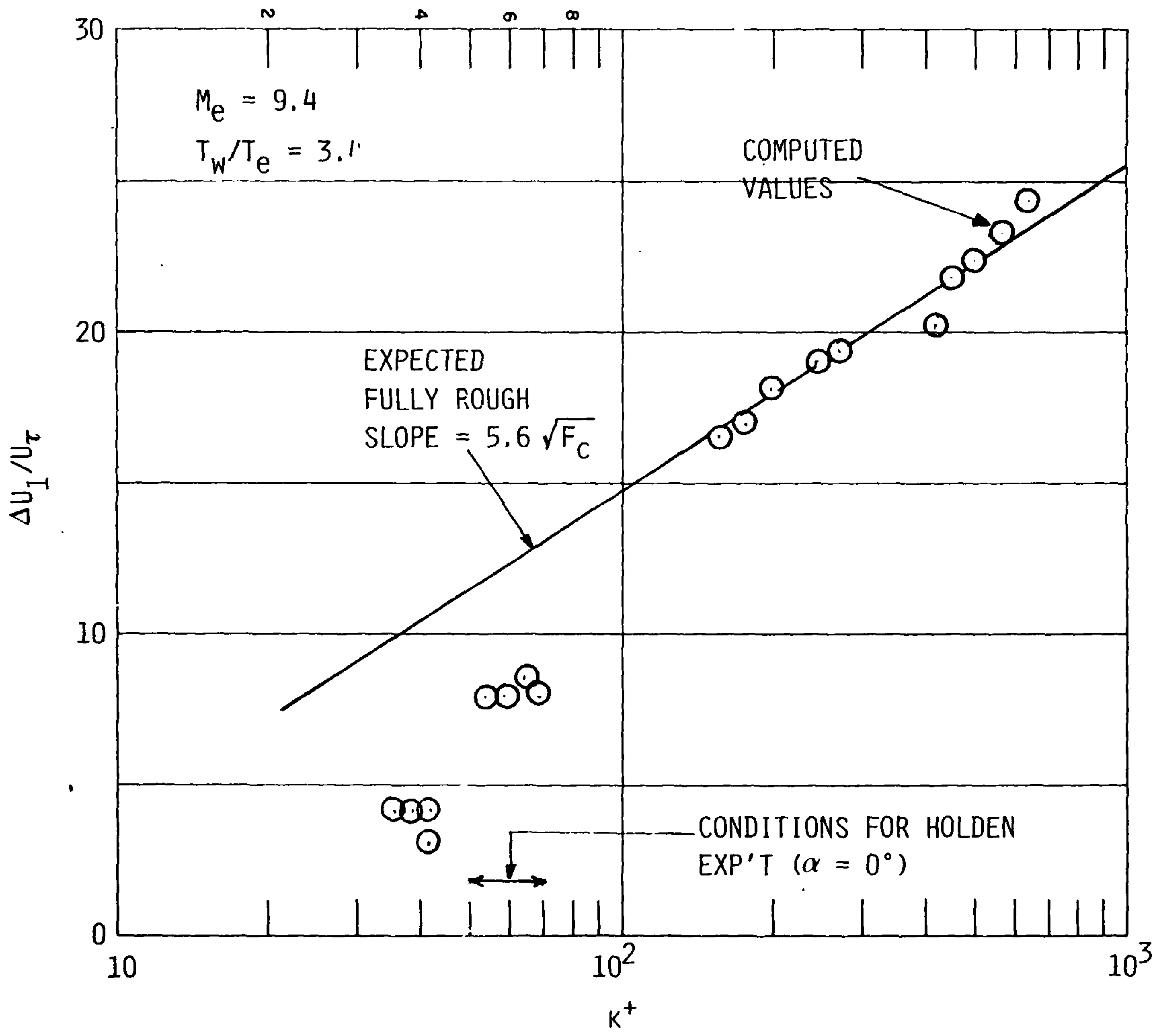

Fig. 24 Computed departure from fully-rough behavior for conditions of Holden's experiment[13] ($M_e = 9.4$).

$$\frac{St}{St_{sm}} = \left(\frac{C_f}{C_{f_{sm}}}\right)^{1/2} \tag{29}$$

Alternatively, the empirical result of Dahm et al.[30] is

$$\frac{St}{St_{sm}} = 1 + 0.6\left(\frac{C_f}{C_{f_{sm}}} - 1\right) \tag{30}$$

In Fig. 25 we show the computed Stanton numbers and skin friction coefficients for various cases spanning variations in roughness height, roughness shape and Mach number. The scatter of computer points may be partially indicative of the inherent numerical accuracy of our computer model, although the points showing the largest departure from the mean generally correspond to upstream locations, where the solution still reflects initial conditions.

The Dahm result, Eq. (30), is seen to provide an excellent fit to the computer solutions, particularly at small augmentation ratios. The square root law of Eq. (29) has an appropriate functional dependence, but consistently underpredicts the computed heating augmentation. A better curve fit to the various computed points shown in Fig. 25 is a combination of the functional dependence of Eqs. (29) and (30):

$$\frac{St}{St_{sm}} = 1 + 1.45\left(\sqrt{\frac{C_f}{C_{f_{sm}}}} - 1\right) . \tag{31}$$

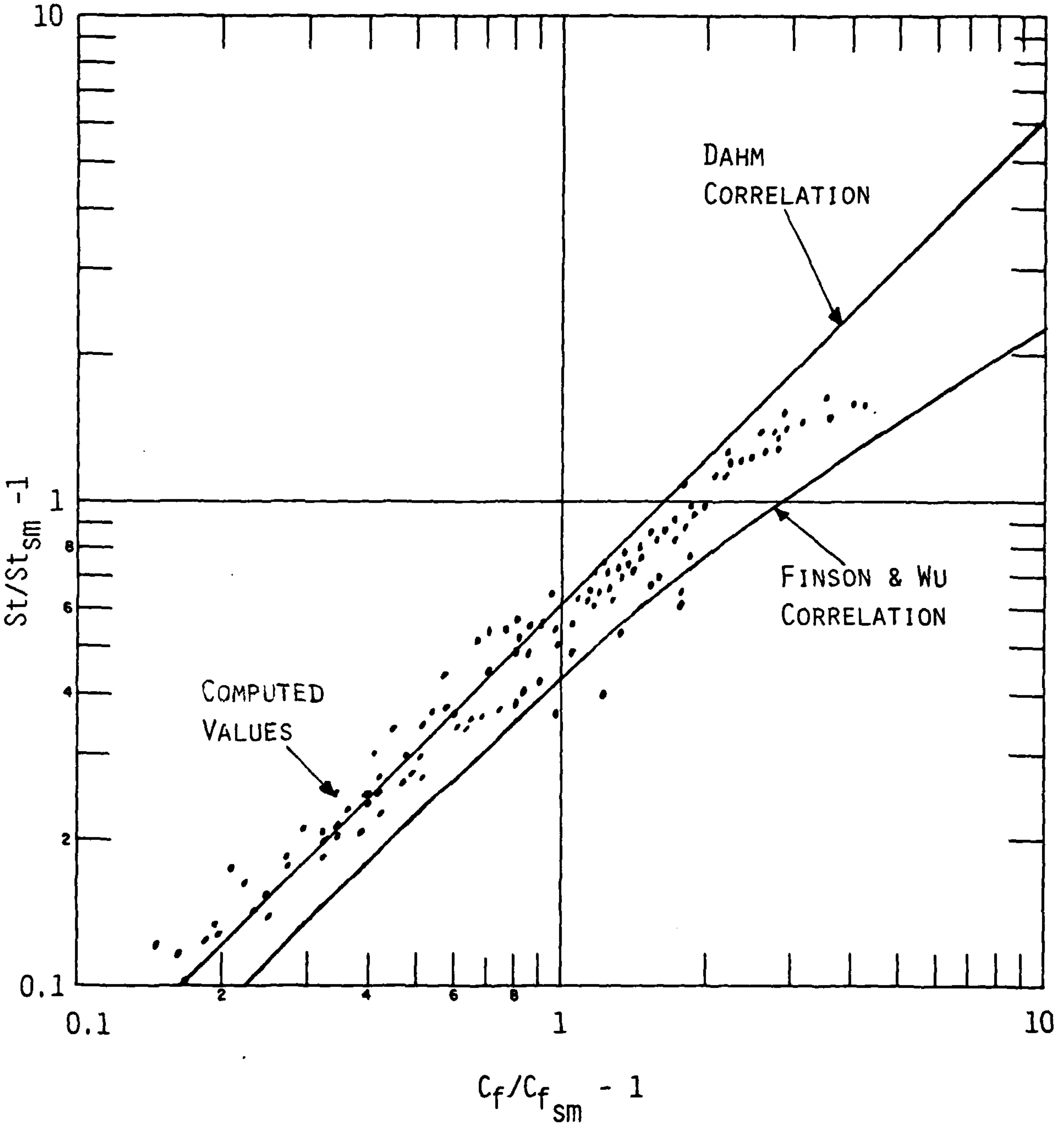

Fig. 25 Computed heat transfer augmentation versus skin friction augmentation.

LIST OF SYMBOLS

B	Rough/smooth transition parameter
$B(y)$	$1-\pi D^2/4\ell^2$
C	Constant in Eq. (16)
C_D	Drag coefficient
C_f	Local skin friction coefficient
D	Roughness element diameter
$f(\lambda)$	Roughness density function [Eq. (5)]
$f(y)$	Roughness blockage function [Eq. (10)]
F_c, F_θ	Compressibility transformation factors [Eq. (20)]
h	Static enthalpy
H	Total enthalpy
k	Roughness element height
k_s	Sandgrain roughness height
k^+	$U_\tau k/\nu_w$
ℓ	Roughness element spacing
L_p	Average peak separation in profilometer trace
M	Mach number
p	Static pressure
R	Pipe radius
Re	Reynolds number
St	Stanton number, $\dot{q}/\rho_e u_e(H_e-h_w)$
T	Temperature
U	Streamwise velocity
U_R	Roughness plateau velocity
ΔU_1	Shift in logarithmic velocity due to roughness
ΔU_3	Shift in logarithmic velocity due to compressibility
U_τ	Friction velocity, $\sqrt{\tau_w/\rho_w}$
V	Normal velocity
X	Streamwise coordinate
y	Normal coordinate

LIST OF SYMBOLS (Cont.)

γ	Ratio of specific heats
δ	Boundary layer thickness
δ^*	Boundary layer displacement thickness
θ	Boundary layer momentum thickness
λ	Piper flow friction factor [Eq. (1)]
λ	[Roughness base area/unit area]$^{-1}$
λ_k	[Roughness frontal area/unit area]$^{-1}$
μ	Dynamic viscosity
ν	Kinematic viscosity, μ/ρ
ρ	Density
Φ	Dissipation function
Ψ	Stream function

Subscripts

e	Boundary layer edge
i	Incompressible
ref	Reference
sm	Smooth
w	Wall
∞	Free stream

Superscripts

*	Based on $k/\theta = 1$

REFERENCES

1. Nikuradse, J., "Stromungsgesetze in rauhen Rohren," VDI Forschungsheft, No. 361, SerB, Vol. 4, (1933); English Translation, NACA TM1292, 1950.

2. Dipprey, D. F. and Sabersky, R. H., "Heat and Momentum Transfer in Smooth and Rough Tubes at Various Prandtl Numbers," International Journal of Heat and Mass Transfer, Vol. 6, 1963, pp. 329-353.

3. Healzer, J. M., Moffat, R. J. and Kays, W. M., "The Turbulent Boundary Layer on a Rough, Porous Plate: Experimental Heat Transfer with Uniform Blowing," Thermosciences Division, Department of Mechanical Engineering, Stanford University, Report No. HMT-18, May 1974.

4. Moffat, R. J. and Kays, W. M., "The Turbulent Boundary Layer on a Porous Plate: Experimental Heat Transfer with Uniform Blowing and Suction," Report No. HMT-1, Thermosciences Division, Dept. of Mech. Eng., Stanford University, 1967.

5. Pimenta, M. M., "The Turbulent Boundary Layer: An Experimental Study of the Transport of Momentum and Heat with the Effect of Roughness," Ph. D. Dissertation, Dept. of Mech. Eng., Stanford University, 1975.

6. Bettermann, D., "Contribution a l'Etude de la Connection Forces Turbulente le Long de Plaques Rugueuses," Int. J. Heat & Mass Transfer 9, 153-164 (1966).

7. Antonia, R. A. and Luxton, R. E., "The Response of a Turbulent Boundary Layer to a Step Change in Surface Roughness. Part 1. Smooth to Rough," Journal of Fluid Mechanics, Vol. 48, 1971, pp. 721-761. Also, Vol. 53, 1972, pp. 737-757.

8. Jackson, M. D. and Baker, D. L., "Passive Nosetip Technology (PANT) Program Interim Report," Vol. III, Part I, SAMSO-TR-74-86, Jan. 1974, Acurex Corp., Mountain View, Calif.

9. Holden, M. S., private communication, 1981.

10. Keel, A. G., Jr., "Influence of Surface Roughness on Skin Friction and Heat Transfer for Compressible Turbulent Boundary Layers," AIAA Paper 77-178, (1977).

11. Voisinet, R. L. P., "Combined Influence of Roughness and Mass Transfer on Turbulent Skin Friction at Mach 2.9," AIAA Paper 79-0003, 1979.

12. Hill, J. A. F., "Measurements of Surface Roughness Effects in the Heat Transfer to Slender Cones at Mach 10," AIAA Paper 80-0345 (1980).

13. Holden, M. S., "Experimental Studies of Sur-face Roughness, Entropy Swallowing and Boundary Layer Transition Effects on the Skin Friction and Heat Transfer Distribution in High Speed Flows," AIAA Paper 82-0034, 1982.

REFERENCES (Cont.)

14. Schlichting, H., "Experimental Investigation of the Problem of Surface Roughness," NACA TM823 (1937). Also Boundary Layer Theory, McGraw-Hill, New York (1968).

15. Chen, C. K. and Roberson, J. A., "Turbulence in Wakes of Roughness Elements," Proceedings of the ASCE, Vol. 100, No. HY1, 1974, pp. 53-67.

16. Raupach, M. R., Thom, A. S., and Edwards, I., "A Wind-Tunnel Study of Turbulent Flow Close to Regularly Arrayed Rough Surfaces," Boundary-Layer Meteorology, Vol. 18, 1980, pp. 373-397.

17. Mirajgaoker, A. G. and Charlu, K. L., "Natural Roughness Effects in Rigid Open Channels," Proceedings of the ASCE, Vol. 89, No. HY5, 1963, pp. 29-44.

18. Sayre, W. W. and Albertson, M. L., "Roughness Spacing in Rigid Open Channels," Proceedings of the ASCE, Vol. 87, No. HY3, 1961, pp. 121-150.

19. O'Loughlin, E. M. and Annambhotla, V. S. S., "Flow Phenomena Near Rough Boundaries," Journal of Hydraulic Research, Vol. 7, 1969, pp. 231-250.

20. Mulhearn, P. J. and Finnigan, J. J., "Turbulent Flow Over a Very Rough, Random Surface," Boundary-Layer Meteorology, Vol. 15, 1978, pp. 109-132.

21. Thom, A. S., "Momentum Absorption by Vegetation," Quarterly Journal of the Royal Meteorology Society, Vol. 97, 1971, pp. 414-428.

22. Seginer, I., Mulhearn, P. J., Bradley, E. F., and Finnigan, J. J., "Turbulent Flow in a Model Plant Canopy," Boundary-Layer Meteorology, Vol. 10, 1976, pp. 423-453.

23. Foster, T., Read, D., and Murray, A., "Reduced Data Report: Surface Roughness Heating Augmentation Tests in AEDC Tunnel F., Vol. II," Acurex Report TR-79-183 (1979).

24. Dvorak, F. A., "Calculation of Turbulent Boundary Layers on Rough Surfaces in Pressure Gradient," AIAA Journal, Vol. 7, No. 9, Sept. 1969, pp. 1752-1759.

25. Dvorak, F. A., "Calculation of Compressible Turbulent Boundary Layers with Roughness and Heat Transfer," AIAA Journal, Vol. 10, No. 11, Nov. 1972, pp. 1447-1451.

26. Simpson, R. L., "A Generalized Correlation of Roughness Density Effects on the Turbulent Boundary Layer," AIAA Journal, Vol. 11, No. 2, Feb. 1973, pp. 242-244.

27. Chen, K. K., "Compressible Turbulent Boundary-Layer Heat Transfer to Rough Surfaces in Pressure Gradient," AIAA Journal, Vol. 10, No. 5, May 1972, pp. 623-629.

REFERENCES (Cont.)

28. Dirling, R. B., Jr., "A Method for Computing Rough-Wall Heat Transfer Rates for Reentry Nosetips," AIAA Paper 73-763, 1973.

29. Hopkins, E. J., and Inouye, M., "An Evaluation of Theories for Predicting Turbulent Skin Friction and Heat Transfer on Flat Plates at Supersonic and Hypersonic Mach Numbers," AIAA Journal, Vol. 9, No. 6, June 1971, pp. 993-1003.

30. Dahm, T. J. et al., "Passive Nosetip Technolo-gy (PANT II) Program, "SAMSO-TR-77-11, Oct. 1976, Acurex Corp., Mountain View, Calif.

31. Dahm, T. J., "Analysis of AEDC Heat Transfer and Shear Data from Roughened RV Nosetip Models in Hypersonic Flow, Reentry Vehicle Technology Program, Final Report, Vol. III, Part IV," BMO/TR-80-52, Acurex Report FR-80-36/AS, 1980.

32. Owen, P. R. and Thomson, W. R., "Heat Transfer Across Rough Surfaces," J. of Fluid Mech., Vol. 15, 1963, pp. 321-334.

33. Finson, M. L. and Wu, P. K. S., "Analysis of Rough Wall Turbulent Heating with Applications to Blunted Flight Vehicles," AIAA Paper 79-008 (1979).

34. Finson, M. L. and Clarke, A. S., "The Effect of Surface Roughness Character on Turbulent Reentry Heating," AIAA Paper 80-1459, 1980.

35. Lin, T. C. and Bywater, R. J., "The Evaluation of Selected Turbulence Models for High-Speed Rough-Wall Boundary Layer Calculations," AIAA Paper No. 80-0132 (1980).

36. Wilson, N. R. and Shaw, R. H., "A Higher Order Closure Model for Canopy Flow," Journal of Applied Meteorology, Vol. 16, Nov. 1977, pp. 1198-1205.

37. Raupach, M. R. and Thom, A. S., "Turbulence in and Above Plant Canopies," Annual Review of Fluid Mechanics, Vol. 13, 1981, pp. 97-129.